

# UNIVERSITI MALAYSIA PAHANG

## BORANG PENGESAHAN STATUS TESIS

JUDUL: COMPUTATIONAL FLUID FLOW ANALYSIS OF A SIDE MIRROR  
FOR A PASSENGER CAR

SESI PENGAJIAN: 2011/2012

Saya, PRABAGAR A/L MURUKESAVAN,

mengaku membenarkan tesis (Sarjana Muda / ~~Sarjana / Doktor Falsafah~~)\* ini disimpan di perpustakaan dengan syarat-syarat kegunaan seperti berikut:

1. Tesis ini adalah hakmilik Universiti Malaysia Pahang (UMP).
2. Perpustakaan dibenarkan membuat salinan untuk tujuan pengajian sahaja.
3. Perpustakaan dibenarkan membuat salinan tesis ini sebagai bahan pertukaran antara institusi pengajian tinggi.
4. \*\*Sila tandakan (✓)

☐

**SULIT**

(Mengandungi maklumat yang berdarjah keselamatan atau kepentingan Malaysia seperti yang termaktub di dalam AKTA RAHSIA RASMI 1972)

☐

**TERHAD**

(Mengandungi maklumat TERHAD yang telah ditentukan oleh organisasi / badan di mana penyelidikan dijalankan)

☒

**TIDAK TERHAD**

Disahkan oleh:

\_\_\_\_\_  
(TANDATANGAN PENULIS)

\_\_\_\_\_  
(TANDATANGAN PENYELIA)

Alamat Tetap:

**No 5 Jalan Lagong 27/84**  
**Taman Alam Megah**  
**40400 Shah Alam**  
**Selangor Darul Ehsan**

**MUHD.AMMAR NIK MU'TASSIM**  
(Nama Penyelia)

Tarikh: **22 JUNE 2012**

Tarikh: **22 JUNE 2012**

CATATAN: \* Potong yang tidak berkenaan.

- \*\* Jika tesis ini SULIT atau TERHAD, sila lampirkan surat daripada pihak berkuasa/organisasi berkenaan dengan menyatakan sekali tempoh tesis ini perlu dikelaskan sebagai SULIT atau TERHAD.

- ♦ Tesis dimaksudkan sebagai tesis bagi Ijazah Doktor Falsafah dan Sarjana secara Penyelidikan, atau disertasi bagi pengajian secara kerja kursus dan penyelidikan, atau Laporan Projek Sarjana Muda (PSM).

# COMPUTATIONAL FLUID FLOW ANALYSIS OF A SIDE MIRROR FOR A PASSENGER CAR

PRABAGAR S/O MURUKESAVAN

Report submitted in partial fulfillment of the requirements  
for the award of Bachelor of Mechanical Engineering with Automotive Engineering

Faculty of Mechanical Engineering  
UNIVERSITI MALAYSIA PAHANG

JUNE 2012

**UNIVERSITI MALAYSIA PAHANG**  
**FACULTY OF MECHANICAL ENGINEERING**

I certify that the project entitled “Computational Fluid Flow Analysis of a Side Mirror for a Passenger Car” is written by Prabagar s/o Murukesavan. I have examined the final copy of this project and in my opinion; it is fully adequate in terms of scope and quality for the award of the degree of Bachelor of Engineering with Automotive Engineering. I herewith recommend that it be accepted in partial fulfillment of the requirements for the degree of Bachelor of Mechanical Engineering with Automotive Engineering.

---

MS. AT-TASNEEM BINTI MOHD AMIN

Examiner

---

Signature

### **SUPERVISOR'S DECLARATION**

I hereby declare that I have checked this project and in my opinion, this project is adequate in terms of scope and quality of this thesis is qualified for the award of the Bachelor of Mechanical Engineering with Automotive Engineering.

Signature :

Name : MR.MUHD AMMAR NIK MU'TASIM

Position : LECTURER

Date : 22<sup>th</sup> JUNE 2012

### **STUDENT'S DECLARATION**

I hereby declare that the work in this thesis is my own except for quotations and summaries which have been duly acknowledged. The thesis has not been accepted for any degree and is not concurrently submitted for award of other degree.

Signature :

Name : PRABAGAR S/O MURUKESAVAN

MATRIC ID : MH09101

Date : 22<sup>th</sup> JUNE 2012

## DEDICATION

*I specially dedicate this project to my beloved parents  
Mr. Murukesavan and Mrs. Bathmavathi, my supervisor  
and those who have guided and motivated me for this project*

## ACKNOWLEDGEMENT

First and foremost, the deepest sense of gratitude to the God, who guide and gave me the strength and ability to complete this final year project successfully. Infinite thanks I brace upon Him. I would like to express my sincere gratitude to my supervisor Mr. Muhd Ammar Nik Mu'Tasim for his continuous guidance, support and encouragement, which gave me huge inspiration in accomplishing this research. His practice of professional ethics and conducts which encourages me to become confident and competent person to work individually as well as in group.

Furthermore, I like to express a very special thanks to Ms. At-Tasneem binti Mohd Amin, who reviewed and certified that my thesis is fully adequate in terms of scope and quality for the award of the degree of Bachelor of Engineering. Not to forget, thanks to the presentation panels who criticized the outcome of this research besides providing some good suggestions to improve the discussion and conclusion as well. I would also like to express my deepest appreciation to my parents whom always support and continue to motivate me to complete this research and thesis. I also owe a depth of gratitude to my university friends who shared their knowledge and ideas that lead to the completion of this thesis.

Finally, thanks to the individuals who has involved neither directly nor indirectly in succession of this research with thesis writing. Indeed I could never adequately express my indebtedness to all of them. Hope all of them continue to support me and give confidence in my efforts in future. Thank you.

## ABSTRACT

Today, reducing the carbon dioxide emissions is vital. The car industry has a responsibility to reduce the fuel consumption and will thereby reduce carbon dioxide emissions. One of the main questions in the automotive industry is how to go about this. One possibility is to change the propulsion system. Another option is to reduce the aerodynamic drag of the car; the topic of this thesis. The drag is of great importance when it comes to velocities over 60 km/h. There are many parts of the car that contribute to drag. One such part is the side-view mirrors. The mirrors increase the total amount of drag by 2-7 percent. The mirror plays a major role in drag contribution for the entire car and therefore mirror optimization is considered very important. Mirror optimization is not an easy task due to uncertainties in the CFD simulations of a few drag counts which makes it impossible to trust all findings. In order to find a good mirror design, a combination of wind tunnel testing in full scale, and CFD simulations is necessary. Mirror design optimization shows great potential. This thesis describes the evaluation of aerodynamic flow effects of a side mirror towards a passenger car based on the side view using ANSYS Fluent CFD simulation software. The parameters that are found in this research are pressure coefficient, total pressure, drag coefficient and lift coefficient. The pressure coefficient of the side mirror designs is evaluated to analyze the unsteady forces that cause fluctuations to mirror surface and image blurring. The fluctuation also causes drag forces that increase the overall drag coefficient, resulting in higher fuel consumption and emission. There are 3 types of model tested in this research. The model is tested in simulation using the speeds of 16.67m/s (60km/h), 25m/s (90km/h) and 33.33m/s (120km/h). The models are then compared using their drag coefficient and lift coefficient. The results indicate that the half-sphere design shows the most effective design with less pressure coefficient which causes fluctuation and has low drag and lift coefficient.



## ABSTRAK

Hari ini, mengurangkan pengeluaran karbon dioksida adalah penting. Industri kereta mempunyai tanggungjawab untuk mengurangkan penggunaan bahan api dan dengan itu akan mengurangkan pengeluaran karbon dioksida. Salah satu persoalan utama dalam industri automotif adalah bagaimana untuk mendalami penambahbaikan dalam perkara ini. Satu kemungkinan ialah dengan menukar sistem tujahan. Satu lagi pilihan adalah untuk mengurangkan seretan aerodinamik kereta iaitu topik tesis ini. Heret adalah amat penting apabila halaju melebihi 60 km/h. Terdapat banyak bahagian kereta yang menyumbang dalam seretan. Salah satu bahagian adalah cermin pandangan sisi. Cermin ini meningkatkan jumlah seretan sebanyak 2 hingga 7 peratus. Cermin ini memainkan peranan yang penting dalam sumbangan seretan untuk keseluruhan kereta dan oleh itu pengoptimuman cermin sisi dianggap sangat penting. Pengoptimuman cermin sisi bukan satu tugas yang mudah kerana ketidakpastian dalam simulasi CFD menjadikannya mustahil untuk dipercayai semua penemuan. Untuk mencari reka bentuk cermin yang baik, kombinasi ujian terowong angin dalam skala penuh, dan simulasi CFD adalah perlu. Pengoptimuman reka bentuk cermin menunjukkan potensi yang besar. Tesis ini menerangkan penilaian kesan aliran aerodinamik cermin sisi ke arah kereta penumpang berdasarkan pandangan sisi dengan menggunakan simulasi perisian ANSYS Fluent CFD. Parameter yang terdapat dalam kajian ini adalah pekali tekanan, jumlah tekanan, pekali seretan dan pekali daya angkat. Pekali tekanan dinilai mengikut reka bentuk cermin dan tekanan akan menyebabkan getaran permukaan cermin dan kekaburan imej. Getaran juga menyebabkan daya seretan yang meningkatkan pekali seretan keseluruhan, mengakibatkan penggunaan bahan api yang lebih tinggi dan pelepasan. Terdapat 3 jenis model yang diuji dalam kajian ini. Model ini diuji dalam simulasi menggunakan kelajuan 16.67m/s (60km/h), 25m/s (90km/h) dan 33.33m/s (120km/h). Semua model ini kemudian dibandingkan dengan menggunakan pekali seretan dan pekali daya angkat. Keputusan menunjukkan bahawa reka bentuk separuh sfera merupakan reka bentuk yang paling berkesan dengan pekali tekanan yang kurang yang menyebabkan getaran dan mempunyai seretan rendah dan pekali daya angkat rendah.

## TABLE OF CONTENTS

	<b>Page</b>
<b>TITLE</b>	i
<b>EXAMINER DECLARATION</b>	ii
<b>SUPERVISOR DECLARATION</b>	iii
<b>STUDENT DECLARATION</b>	iv
<b>DEDICATION</b>	v
<b>ACKNOWLEDGEMENT</b>	vi
<b>ABSTRACT</b>	vii
<b>ABSTRAK</b>	viii
<b>TABLE OF CONTENTS</b>	ix
<b>LIST OF TABLES</b>	xii
<b>LIST OF FIGURES</b>	xiii
<b>LIST OF SYMBOLS</b>	xv
<b>LIST OF ABBREVIATIONS</b>	xvi
<b>LIST OF APPENDICES</b>	xvii
 <b>CHAPTER 1            INTRODUCTION</b>	
1.1     Background	1
1.2     Problem Statement	2
1.3     Objectives	2
1.4     Scope of Study	3
1.5     Significant of Study	3
1.6     Structure of Report	3
 <b>CHAPTER 2            LITERATURE REVIEW</b>	
2.1     Computational Fluid Dynamics (CFD)	5
2.1.1    CFD Solving Approaches	6
2.2     History of Automotive Aerodynamic Technology	7
2.3     Automotive Aerodynamics	9
2.4     Aerodynamics Drag	10
2.5     Drag Force	11
2.6     Aerodynamic Lift	11
2.7     Aerodynamic Pressure	12
2.8     Drag Coefficient	13
2.9     External Flow	14

2.10	Vortex Shedding	15
2.11	Side view mirror	16
2.11.1	Designs	17

## **CHAPTER 3            METHODOLOGY**

3.1	Introduction	18
3.2	Flow Chart Description	21
3.2.1	Project Introduction	21
3.2.2	Literature Study	21
3.2.3	Problem Solving	21
3.3	Computer Aided Drawings (CAD)	22
3.3.1	Designing of Wind Tunnel	22
3.3.2	Designing of Passenger Car	23
3.3.3	Designing of Side Mirrors	24
3.4	Mesh Generation	26
3.5	Simulation Model	27
3.6	Assumptions Made	28
3.7	Solver Setting	28

## **CHAPTER 4            RESULT AND DISCUSSION**

4.1	Introduction	30
4.2	Critical Points across the side mirror	30
4.3	Pressure Coefficient, $C_p$	31
4.3.1	Pressure Coefficient, $C_p$ for 16.67m/s (60km/h)	31
4.3.2	Pressure Coefficient, $C_p$ for 25m/s (90km/h)	35
4.3.3	Pressure Coefficient, $C_p$ for 33.33m/s (120km/h)	39
4.4	Total Pressure, $P_{Total}$	43
4.4.1	Total Pressure, $P_{total}$ for 16.67m/s (60km/h)	43
4.4.2	Total Pressure, $P_{total}$ for 25m/s (90km/h)	46
4.4.3	Total Pressure, $P_{total}$ for 33.33m/s (120km/h)	48
4.5	Drag Coefficient, $C_D$	50
4.5.1	Drag Coefficient of side mirror models at 16.67m/s (60km/h)	50
4.5.2	Drag Coefficient of side mirror models at 25m/s (90km/h)	51
4.5.3	Drag Coefficient of side mirror models at 33.33m/s (120km/h)	51
4.6	Lift Coefficient, $C_L$	52
4.6.1	Lift Coefficient of side mirror models at 16.67m/s (60km/h)	53
4.6.2	Lift Coefficient of side mirror models at 25m/s (90km/h)	53
4.6.3	Lift Coefficient of side mirror models at 33.33m/s (120km/h)	54

4.7	Discussion	55
-----	------------	----

## **CHAPTER 5            CONCLUSION AND RECOMMENDATION**

5.1	Introduction	56
5.2	Conclusion	56
5.3	Recommendations for Future Research	57

<b>REFERENCES</b>	58
-------------------	----

<b>APPENDICES</b>	60
-------------------	----

**LIST OF TABLES**

<b>Table No.</b>	<b>Title</b>	<b>Page</b>
3.1	Solver Settings	28
3.2	Boundary Condition Settings	29

## LIST OF FIGURES

Figure No.	Title	Page
2.1	The CFD Process flow	6
2.2	History of vehicle dynamic in passenger car	8
2.3	Aerodynamic of bluff bodies	9
2.4	Pressure and velocity gradients in the air flow over the body coefficient	12
2.5	Drag Coefficients of various shapes	14
2.6	Flow around a vehicle	15
2.7	Vortex shedding in flow over a cylindrical body	16
2.8	Different frontal area mirror designs over the years	17
3.1	Methodology flow chart for PSM 1	19
3.2	Methodology flow chart for PSM 2	20
3.3	Virtual Wind Tunnel Design	22
3.4	Front View and Isometric View of Passenger Car Model	23
3.5	Side View of Passenger Car Model	23
3.6	Design of Side Mirror 1	24
3.7	Design of Side Mirror 2	25
3.8	Design of Side Mirror 3	25
3.9	Meshing of wind tunnel and model	26
3.10	Wind Tunnel Boundary Setting	27
4.1	Example of side mirror with 100 critical points	31
4.2	Pressure Coefficient ( $C_p$ ) contour for Model 1 (16.67m/s)	32
4.3	Graph of Pressure Coefficient of 100 critical points across Side Mirror 1 frontal area	32
4.4	Pressure Coefficient ( $C_p$ ) contour for Model 2 (16.67m/s)	33
4.5	Graph of Pressure Coefficient of 100 critical points across Side Mirror 2 frontal area	34
4.6	Pressure Coefficient ( $C_p$ ) contour for Model 3 (16.67m/s)	34
4.7	Graph of Pressure Coefficient of 100 critical points across Side Mirror 3 frontal area	35
4.8	Pressure Coefficient ( $C_p$ ) contour for Model 1 (25m/s)	36
4.9	Graph of Pressure Coefficient of 100 critical points across Side Mirror 1 frontal area	36
4.10	Pressure Coefficient ( $C_p$ ) contour for Model 2 (25m/s)	37
4.11	Graph of Pressure Coefficient of 100 critical points across Side Mirror 2 frontal area	38
4.12	Pressure Coefficient ( $C_p$ ) contour for Model 3 (25m/s)	38

4.13	Graph of Pressure Coefficient of 100 critical points across Side Mirror 3 frontal area	39
4.14	Pressure Coefficient ( $C_p$ ) contour for Model 1 (33.33m/s)	40
4.15	Graph of Pressure Coefficient of 100 critical points across Side Mirror 1 frontal area	40
4.16	Pressure Coefficient ( $C_p$ ) contour for Model 2 (33.33m/s)	41
4.17	Graph of Pressure Coefficient of 100 critical points across Side Mirror 2 frontal area	42
4.18	Pressure Coefficient ( $C_p$ ) contour for Model 3 (33.33m/s)	42
4.19	Graph of Pressure Coefficient of 100 critical points across Side Mirror 3 frontal area	43
4.20	Total Pressure contour for Model 1 (16.67m/s)	44
4.21	Total Pressure contour for Model 2 (16.67m/s)	45
4.22	Total Pressure contour for Model 3 (16.67m/s)	45
4.23	Total Pressure contour for Model 1 (25m/s)	46
4.24	Total Pressure contour for Model 2 (25m/s)	47
4.25	Total Pressure contour for Model 3 (25m/s)	47
4.26	Total Pressure contour for Model 1 (33.33m/s)	48
4.27	Total Pressure contour for Model 2 (33.33m/s)	49
4.28	Total Pressure contour for Model 3 (33.33m/s)	49
4.29	Graph of Drag coefficient ( $C_d$ ) for models (16.67m/s)	50
4.30	Graph of Drag coefficient ( $C_d$ ) for models (25m/s)	51
4.31	Graph of Drag coefficient ( $C_d$ ) for models (33.33m/s)	52
4.32	Graph of Lift coefficient ( $C_L$ ) for models (16.67m/s)	53
4.33	Graph of Lift coefficient ( $C_L$ ) for models (25m/s)	54
4.34	Graph of Lift coefficient ( $C_L$ ) for models (33.33m/s)	54
4.35	Design Comparisons at speed of 33.33m/s	55

**LIST OF SYMBOLS**

%	Percentage
$\rho$	Density
km/h	Kilometer per hour
m/s	Meter per second
m	Meter
V	Velocity
A	Frontal Area
L	Length
kg	Kilogram
m <sup>3</sup>	Meter cube
kPa	Kilo Pascal
P <sub>static</sub>	Static Pressure
P <sub>dynamic</sub>	Dynamic Pressure
P <sub>atm</sub>	Atmospheric Pressure
P <sub>Total</sub>	Total Pressure
C <sub>D</sub>	Drag Coefficient
C <sub>L</sub>	Lift Coefficient
F <sub>D</sub>	Drag Force
F <sub>L</sub>	Lift Force
k- $\epsilon$	K-Epsilon



**LIST OF ABBREVIATIONS**

2D	Two Dimensional
3D	Three Dimensional
ANSYS	Analysis System
CAA	Computational Aero Acoustics
CFD	Computational Fluid Dynamics
DNS	Direct Numerical Simulations
FEM	Finite Element Method
FVM	Finite Volume Method
FYP	Final Year Project
LES	Large Eddy Simulations
RANS	Reynolds Averaged Navier-Stokes

**LIST OF APPENDICES**

<b>Appendix</b>	<b>Title</b>	<b>Page</b>
A1	Gantt chart for Final Year Project 1	60
A2	Gantt chart for Final Year Project 2	61
B1	Data of Drag Coefficient (16.67m/s)	62
B2	Data of Drag Coefficient (25m/s)	63
B3	Data of Drag Coefficient (33.33m/s)	64
C1	Data of Lift Coefficient (16.67m/s)	65
C2	Data of Lift Coefficient (25m/s)	66
C3	Data of Lift Coefficient (33.33m/s)	67

## **CHAPTER 1**

### **INTRODUCTION**

#### **1.1 BACKGROUND**

Reducing fuel consumption, and therefore reducing the carbon dioxide emissions, is one of the most important goals in today's car industry. One way this can be achieved is by reducing the engine size, using an electric motor with a combustion engine, reducing the weight of the car and reducing the aerodynamic drag of the car. The latter is of great importance when it comes to velocity over 60km/h. Above this velocity, the aerodynamic resistance is higher than the rolling resistance (Versteeg, H.K., 2007). Streamlined body design in a passenger car helps reducing the aerodynamic drag and eventually improves the engine mileage. On the contrary, accessories attached to the body skin of a car cause the unfavorable aerodynamic examples. In order to obtain the rear sight, unfortunately the mirror does not pay only the aerodynamic penalty which increases body form drag, but also causes the acoustic noise thus causes mirror fluctuations to the cabin crews.

While the aerodynamic body styling of the passenger car has been upgraded with a lot of efforts, the defects caused by important accessory such as the side view mirror have been ignored. The main stream meets a side flow which has the flow direction tangent to the windshield surface near the A-pillar. And a conical vortex sheet is generated along the pillar and merges into the mainstream. Therefore, very complicate flow pattern appears by combining these flow patterns near the driver side window. Moreover, since the side mirror is mounted on the driver door near hinge, the wake flow behind this obstacle become much complicated. (D. Gillespie, 2000)

## **1.2 PROBLEM STATEMENT**

Reducing fuel consumption, and therefore reducing the carbon dioxide emissions, is one of the most important goals in today's car industry. One way this can be achieved is by reducing the aerodynamic drag of the car. It is a great importance when it comes to velocities over 60km/h. Above this velocity, the aerodynamic resistance is higher than the rolling resistance. Streamlined body design in a passenger car helps reducing the aerodynamic drag and eventually improves the engine mileage. (H.K. Versteeg, 2007).

On the contrary, accessories attached to the body skin of a car cause the unfavorable aerodynamic examples. In order to obtain the rear sight, unfortunately the mirror does not pay only the aerodynamic penalty which increases body form drag, but also causes the acoustic noise and the mirror fluctuations to the cabin crews.

The main function of rear mirror is to provide drivers the rear view of a vehicle. Rear view side mirror contributes to aerodynamic drag, noise and vibration. The aerodynamic drag can be reduced to lower the fuel consumption rate.

## **1.3 OBJECTIVES**

The objectives of the project are as follows:

- i. To study the effects of aerodynamic flow towards a passenger car side mirror based on the side view (x-y axis)
- ii. To compare different types of side mirror designs using CFD
- iii. The best design which has better flow characteristics is chosen as a base model.

## **1.4 SCOPES OF STUDY**

The scopes of the project are as follows:

- i. Designing a full scale of the side mirror structure attached to a passenger car model.
- ii. Design 3 new designs of side mirror for comparisons.
- iii. Run analysis using a CFD application which is ANSYS Fluent to obtain results by using different speed (km/h) parameter.
- iv. Compare the obtained computational results with experiment method results by F. Alam Et.Al., 2007.

## **1.5 SIGNIFICANT OF STUDY**

Computational Fluid Dynamics (CFD) is done to save cost and time of running high cost experiments using experimental wind tunnel. The research could reduce the consumption of fuel and produce less harmful emissions to the atmosphere during the usage of automobiles. From this research, it will help to increase the importance of usage of computational results to analysis a certain experiment with high cost and long duration.

## **1.6 STRUCTURE OF REPORT**

This report consists of five chapters. The first chapter is introduction about the research study. It includes the background of study, problem statement, objectives, scopes, significant of the study and the structure of report.

Next chapter focuses on the literature review based on the previous aerodynamic experiments done. Besides that, this chapter includes the fundamental of aerodynamic, the factors that influence aerodynamic and parameters associated with the aerodynamic effect assessment. So, this chapter has major influences to increase better understanding on this research study and is very helpful to design the methodology of study.

Chapter 3 describes the methodology of the procedures of this research which was done. The flow chart of this research is presented with potential arising issues with the preventive action plans. The methods and procedures are described in general. The designing of wind tunnel, passenger car and side mirror are explained. Besides that, the details of used simulation settings and boundary conditions are briefly described. Other than that, the data analysis method is also explained at the end of this chapter.

The results and discussions are presented in next chapter. The generated data of pressure coefficient, total pressure, drag coefficient and lift coefficient are presented in form of graphics for qualitative discussion. The contours of flow are also discussed to understand the best design characteristics. The correlation between the experiment result and simulation result is also discussed. Finally, the outcome of this study was compared with previous wind tunnel experiment done by researches.

The final chapter of this thesis consists of conclusion of this research study. The overall conclusion with finalized details is discussed with some recommendation for improvements proposed.

## **CHAPTER 2**

### **LITERATURE REVIEW**

#### **2.1 COMPUTATIONAL FLUID DYNAMICS (CFD)**

Computational fluid dynamics (CFD) is a computer simulation that analyzes systems for fluid flows, heat transfer, and phenomena such as chemical reactions. The rapid development of computational power and CFD technique, the field of Computational Aero Acoustics (CAA) becomes more and more relevant to the industrial applications, and this method has been applied in the area of the aerospace industry , meteorology (weather prediction), and external environment of buildings (wind loads and ventilation) commonly. CFD has many advantages over experiment-based approaches, such as reduction of lead times and costs of new designs, study systems under hazardous conditions, systems that are impossible to study with controlled experiments and, the unlimited level of detail of the results.

There are also problems with CFD. The physics are complex and the result from CFD is only as good as the operator and the physics embedded. With today's computer power, there is a limitation of grid fineness and the choice of solving approach (DNS, LES and turbulence model). This can result in errors, such as numerical diffusion, false diffusion and wrongly predicted flow separations. The operator must then decide if the result is significant. While presently, CFD is no substitute for experimentation, it is a very helpful and powerful tool for problem solving.

Concerning the comfort of driver, more and more attention is paid to noise in the car development process. Flow induced noise, generated by additional device at the

vehicle body, i.e. Side mirrors, antennas or spoilers are especially important. (H. K. Versteeg, 2007)

When working with CFD a number of different steps are followed. These steps are illustrated in figure 2.1.

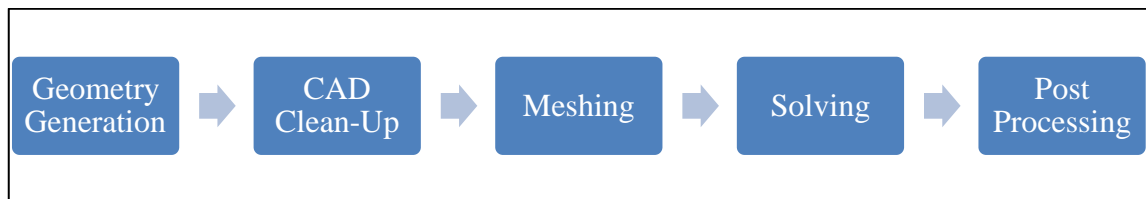


**Figure 2.1:** The CFD process flow

The first step is to create geometry (with CAD). This is often already done by other departments or done by scanning a model. The geometry cannot have any holes, it has to be airtight, and unnecessary things in the CAD model that do not affect the flow has to be removed to save computer power. This is called CAD cleanup. The next step is to generate a mesh and this is often done automatically by a meshing program. Then the flow is simulated by a solver. After the simulation is ready, it is time for post processing. Post processing involves getting drag and lift data, and analyzing the flow.

### 2.1.1 CFD solving approaches

There are many types of solving approach, one of that is the Direct Numerical Simulations (DNS). It solves the Navier-Stokes equation numerically. This will resolve all the different turbulent scales. The solution will be transient and requires a very fine mesh with sufficiently small time steps. Due to the extreme grid size and number of time steps required for a simulation at high Reynolds number, this approach is not today possible (lack of computer power).

Then there is the Reynolds-Averaged Navier-Stokes (RANS) method. It gives an approximate time-averaged solution to the Navier-Stokes equation and focuses on the mean flow properties. The fluctuating velocity field, also called Reynolds stress, has to be modeled. But this turbulence model cannot solve all turbulence scales.





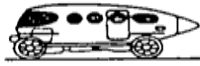












The last approach used in this experiment is the Large Eddy Simulations (LES) it computes the larger eddies in a time-dependent simulation while the universal behavior of the smaller eddies can be captured with a model. LES uses a spatial filtering operation to separate the larger and the smaller eddies. (D. Gillespie, 2000)

## **2.2 HISTORY OF AUTOMOTIVE AERODYNAMICS TECHNOLOGY**

Aerodynamics and vehicle technology have merged only very slowly. A synthesis of the two has been successful only after several tries. This is surprising since in the neighboring disciplines of traffic technology, naval architecture, and aeronautics the cooperation with fluid mechanics turned out to be very fruitful. Of course, the designers of ships and airplanes were in a better position. They found their originals in nature from fish and birds. From these natural shapes they took many essential features. The automobile had no such originals. Hence its designers tried to borrow shapes from ships and airplanes, which must have appeared progressive to them. Very soon this turned out to be the wrong approach. Only when it broke away from these improper originals did aerodynamics make a breakthrough in the automobile.

Another reason for the early repeated failures of aerodynamics with vehicles is that it started far too early. The first automobiles were pretty slow. On the bad roads of those days streamlined bodies would have looked ridiculous. Protecting driver and passengers from wind, mud and rain could be accomplished very well with the traditional design of horse-drawn carriages. Later the prejudice that streamlined bodies were something for odd persons overrode the need for making use of the benefits of aerodynamics for economical reasons. A brief overview of the history of vehicle aerodynamics is summarized in Figure 2.2.

During the first two of the total four periods, aerodynamic development was done by individuals, most of them coming from outside the car industry. They tried to carry over basic principles of aircraft aerodynamics to cars. Later, during the remaining two periods, the discipline of vehicle aerodynamics was taken over by the car companies and was integrated into product development. Since then, teams, not individual inventors, have been responsible for aerodynamics.

Basic shapes	1900 to 1925	 Torpedo	 Boat tail	 Air ship
Streamlined cars	1921 to 1923	 Rumpler		 Bugatti
	1922 to 1939	 Jaray 		
	1934 to 1939	 Kamm		 Schlör
	Since 1955	 Citröen		 NSU-Ro 80
Detail optimization	Since 1974	 VW-Scirocco I		 VW-Golf I
Shape optimization	Since 1983	 Audi 100 III		 Ford Sierra

**Figure 2.2:** History of vehicle dynamic in passenger car

Source: D. Gillespie (2000)

The first automobile to be developed according to the aerodynamic principles was a torpedo-shaped vehicle that had given it a low drag coefficient but the exposed driver and out of body wheels must have certainly disturbed its good flow properties. However they ignored the fact that the body was close to the ground in comparison to aircrafts and underwater ships flown in a medium that encloses the body. In a car like this, the ground along with the free-standing wheels and the exposed undercarriage causes disturbed flow. As the years pass the studies on aerodynamic effects on cars increase and the designs are being developed to accommodate for the increasing needs and for economic reasons. The wheels developed to be designed within the body, lowering as a result the aerodynamic drag and produce a more gentle flow. The tail was for many years long and oddly shaped to maintain attached the streamline. The automobiles became developed even more with smooth bodies, integrated fenders and headlamps enclosed in the body. The designers had achieved a shape of a car that differed from the

traditional horse drawn carriages. They had certainly succeeded in building cars with low drag coefficient (D. Gillespie, 2000)

### 2.3 AUTOMOTIVE AERODYNAMICS

Aerodynamics of cars became more and more important with the increase of their velocity. In the beginning of the 20th century, the shape of vehicles was adopted from the field of aviation and ships. Cars had an aerodynamic shape but their velocity was very low, mainly due to the quality of the roads. Aerodynamics is the branch of dynamics that deals with the motion of air and other gaseous fluids and with the forces acting on bodies in motion relative to such fluids. Automotive aerodynamics is the study of the aerodynamics of road vehicles. The main concerns of automotive aerodynamics are reducing drag, reducing wind noise, minimizing noise emission and preventing undesired lift forces at high speeds. For some classes of racing vehicles, it may also be important to produce desirable downwards aerodynamic forces to improve traction and thus cornering abilities (D. Gillespie, 2000). An aerodynamic automobile will integrate the wheel and lights in its shape to have a small surface. It will be streamlined, for example it does not have sharp edges crossing the wind stream above the windshield and will feature a sort of tail called a fastback or Kammback or lift back. It will have a flat and smooth floor to support the venturi or diffuser effect and produce desirable downwards aerodynamic forces. The air that rams into the engine bay, is used for cooling, combustion, and for passengers, then reaccelerated by a nozzle and then ejected under the floor. Most everyday things are either caused by aerodynamic effects or in general obey the aerodynamic laws. For aerodynamic bodies a simplified procedure may then be devised for the evaluation of the aerodynamic loads.

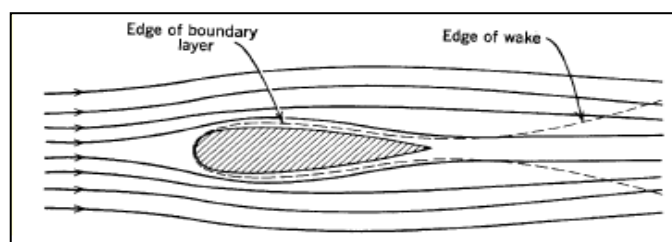


**Figure 2.3:** Aerodynamic of bluff bodies

Source: D. Gillespie (2000)

A car driven in a road is affected by aerodynamic forces created. The aerodynamics of such cars is of vital importance. They affect the cars stability and handling. They influence both performance and safety.

## 2.4 AERODYNAMICS DRAG

The force on an object that resists its motion through a fluid is called drag. When the fluid is a gas like air, it is called aerodynamic drag (or air resistance). When the fluid is a liquid like water it is called hydrodynamic drag. Drag is a complicated phenomena and explaining it from a theory based entirely on fundamental principles is exceptionally difficult.

Fluids are characterized by their ability to flow. In semi-technical language, a fluid is any material that can't resist a shear force for any appreciable length of time. This makes them hard to hold but easy to pour, stir, mix, and spread. As a result, fluids have no definite shape but take on the shape of their container. Fluids are unusual in that they yield their space relatively easy for other material things at least when compared to solids. Fluids may not be solid, but they are most certainly material. The essential property of being material is to have both mass and volume. Material things resist changes in their velocity and no two material things may occupy the same space at the same time. The portion of the drag force that is due to the inertia of the fluid is the resistance to change that the fluid has to be pushed aside so that something else can occupy its space is called the pressure drag. (A. Cengel, 2006)

$$C_d = \frac{F_d}{\frac{1}{2}\rho v^2 A} \quad (2.1)$$

Based on Eq. (2.1), where  $F_d$  is the Drag force,  $C_D$  is the Drag coefficient,  $\rho$  is the fluid density,  $A$  is the frontal area and  $v$  is the Velocity.

## 2.5 DRAG FORCE

The drag equation for an object moving through a fluid is as followed

$$F_d = \frac{1}{2} \rho v^2 C_d A \quad (2.2)$$

Based on Eq. (2.2), where  $F_d$  is the force of the drag,  $\rho$  is the density,  $v$  is the velocity,  $C_d$  is the drag coefficient and  $A$  is the reference area. The most important variables are the reference area (frontal area of the car) and the drag coefficient. By reducing these, the aerodynamic drag will be reduced which will lead to lower fuel consumption rate.

## 2.6 AERODYNAMICS LIFT

Lift is normally of little importance in passenger cars as their speed is usually too low to produce much lift. It was noticed early on that something strange happened at high speeds: the car seemed to be lifting off the ground. The lift can be serious, particularly in racing cars. It has a serious effect on the control and handling of the car. (A. Cengal, 2006)

Lift occurs because the airflow over the top of a car is faster than across the bottom. This occurs to some degree in all cars. As the speed increases, the pressure decreases, according to Bernoulli's theorem. The top of the car therefore has a lower pressure than the bottom, and the result is a lifting force. The amount of lift generated by an object depends on a number of factors, including the density of the air, the velocity between the object and the air, the viscosity and compressibility of the air, the surface area over which the air flows, the shape of the body, and the body's inclination to the flow, also called the angle of attack.

$$C_L = F_L / (1/2 \rho V^2 A) \quad (2.3)$$

Based on Eq. (2.3), where  $F_L$  is the lift force,  $C_L$  is the Lift coefficient,  $\rho$  is the fluid density and  $A$  is the frontal area, while  $v$  is the velocity

## 2.7 AERODYNAMIC PRESSURE

The gross flow over the body of a vehicle is governed by the relationship between velocity and pressure expressed in Bernoulli's Equation. Bernoulli's Equation assumes incompressible flow which is reasonable for automotive aerodynamics. (A. Cengel, 2006)

$$P_{static} + P_{dynamic} = P_{total} \quad (2.4)$$

$$P_s + \frac{1}{2} \rho V^2 = P_t \quad (2.5)$$

Based on Eq. (2.4) and Eq. (2.5), where  $\rho$  is the density of air in  $\text{kg/m}^3$  and  $V$  is the velocity of air (relative to the car) in  $\text{m/s}$

In the equation above, the sum of the forces brings in the pressure affect acting on the incremental area of the body of fluid. The static plus the dynamic pressure of the air will be constant ( $P_t$ ) as it approaches the vehicle. At the distance from the vehicle the static pressure is simply the ambient, or barometric, pressure ( $P_{atm}$ ). The dynamic pressure is produced by the relative velocity, which is constant for all streamlines approaching the vehicle. As the flow approaches the vehicle, the streamlines split, some going above the vehicle and others below. By inference, one streamline must go straight to the body and stagnate (impinging on the bumper of the vehicle). At that point the relative velocity has gone to the zero. This will make the static pressure observed at that point on the vehicle. Figure 2.4 below shows flow over a cylinder that it affects is most same to the vehicle's coefficient. (D. Gillespie, 2000)

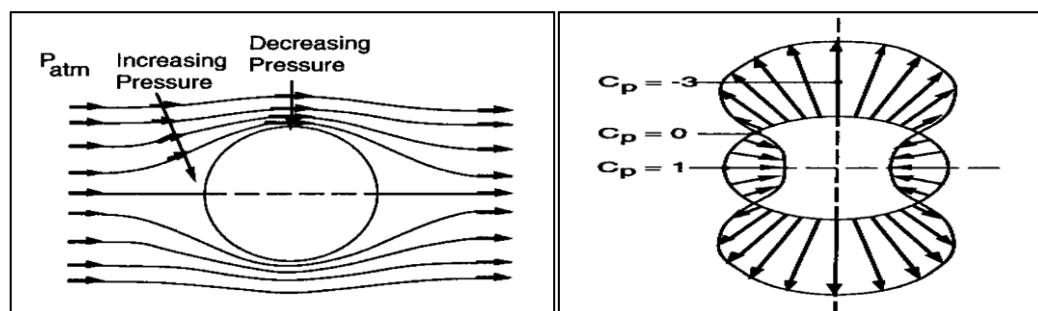


**Figure 2.4:** Pressure and velocity gradients in the air flow over the body coefficient

Source: D. Gillespie, (2000)

The static pressure will distribute along the body of a car. The pressures are indicated as being negative or positive with to the ambient pressure some distance from the vehicle. A negative pressure is developed at the front edge of the hood as the flow rising over the front of the vehicle attempts to turn and follow horizontally along the hood (A. Cengal, 2006). Near the base of the windshield and cowl, the flow must be turned upward, thus the high pressure is experienced. Over the roof line the pressure goes negative as the air flow tries to follow the roof contour.

## 2.8 DRAG COEFFICIENT

The aerodynamic drag coefficient is a measure of the effectiveness of a streamline aerodynamic body shape in reducing the air resistance to the forward motion of a vehicle. A low drag coefficient implies that the streamline shape of the vehicle's body is such as to enable it to move easily through the surrounding viscous air with the minimum of resistance, conversely a high drag coefficient is caused by poor streamlining of the body profile so that there is a high air resistance when the vehicle is in motion.

The aerodynamic drag is the focus of public interest in vehicle aerodynamics. It is and even more so it's non-dimensional number of  $C_D$ , the drag coefficient has almost become a synonym for the entire discipline. Performance, fuel economy, emissions, and top speed are important attributes of a vehicle because they represent decisive sales arguments, and they all are influenced by drag. Drag coefficient ( $C_D$ ) is a commonly published rating of a car's aerodynamic smoothness, related to the shape of the car. Multiplying  $C_D$  by the car's frontal area gives an index of total drag. The result is called drag area, and is listed below for several cars. The width and height of curvy cars lead to gross overestimation of frontal area. The aerodynamic drag coefficient equation is (D. Gillespie, 2000)

$$C_D = \frac{F_D}{\frac{1}{2} \rho V^2 A} \quad (2.6)$$

Based on Eq. (2.6), where  $F_D$  is the drag force in [N],  $\rho$  is the density of the air in [ $\text{kg}/\text{m}^3$ ],  $A$  is the area of the body in [ $\text{m}^2$ ] and  $V$  is the velocity of the body in [ $\text{m}/\text{s}$ ]

The drag coefficient varies over a broad range with different shapes. Figure 2.5 below shows the coefficients for a number of shapes. In each case it is presumed that the air approaching the body has no lateral component. The simple aerofoil has a drag coefficient of 0.007. This coefficient means that the drag force is 0.007 times as large as the dynamic pressure acting over the area of the plate.

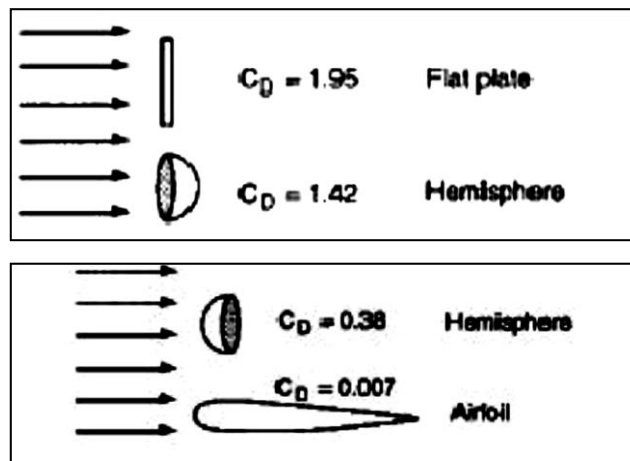


**Figure 2.5:** Drag coefficients of various shapes

Source: A. Cengel, (2006)

In contrast, with the much better aerodynamic design of cars, their drag coefficient is not as sensitive to yaw angle because the flow will not separate so readily. Normally, the drag coefficient increase by 5% to 10% with yaw angles in the range typical of on-road driving for passenger cars. The difference of yaw angle will influence on the drag coefficients of several different types of vehicles (A. Cengel, 2006).

## 2.9 EXTERNAL FLOW

The flow around a vehicle is responsible for its directional stability as well as straight line stability, dynamic passive steering, and response to crosswind depend on the external flow field. Furthermore, the outer flow should be tuned to prevent droplets of rain water from accumulating on windows and outside mirrors, to keep headlights free of dirt, to reduce wind noise, to prevent the windshield wipers from lifting off, and to cool the engine's oil pan, muffler, and brakes, etc. The external flow around a vehicle



is shown in Figure 2.6 below. In still air, the undisturbed velocity,  $V$  is the road speed of the car. Provided no flow separation takes place, the viscous effects in the fluid are restricted to a thin layer of a few millimeters thickness, called the boundary layer.

Beyond this layer the flow can be regarded as inviscid, and its pressure is imposed on the boundary layer. Within the boundary layer the velocity decreases from the value of the inviscid external flow at the outer edge of the boundary layer to zero at the wall, where the fluid fulfills a no slip condition. When the flow separates, the boundary layer is "dispersed" and the flow is entirely governed by viscous effects. The character of the viscous flow around a body depends only on the body shape and the Reynolds number. For different Reynolds numbers entirely different flows may occur for one and the same body geometry. Thus the Reynolds number is the dimensionless parameter which characterizes a viscous flow (Heisler. H., 2002)

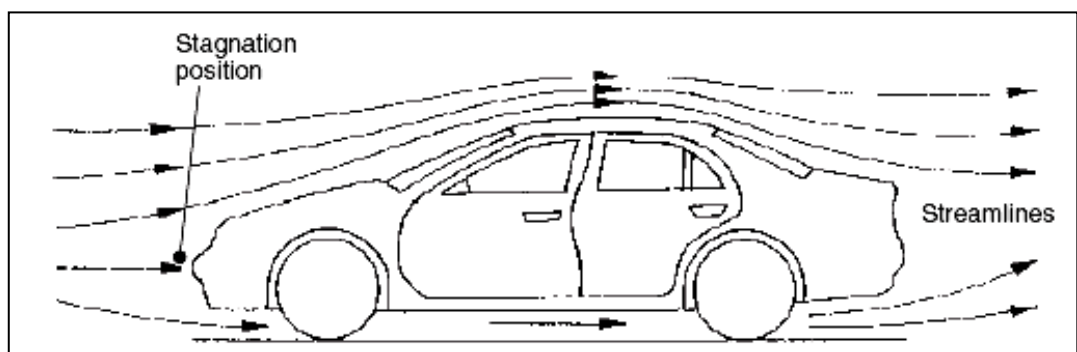


**Figure 2.6:** Flow around a vehicle

Source: Heisler. H., (2002)

## 2.10 VORTEX SHEDDING

Vortex shedding is an unsteady flow that takes place at special flow velocities (according to the size and shape of the cylindrical body). In this flow, vortices are created at the back of the body and periodically from both sides of the body. Vortex shedding is caused when air flows past a blunt structure. The air flow past the object creates alternating low-pressure vortices on the downwind side of the object. The object will tend to move towards the low pressure zone. Eventually, if the frequency of vortex

shedding matches the resonant of the structure, the structure will begin to resonate and the movement of the structure can become self sustaining.

As the Reynolds number (for flow over spherical bodies) increases above 20, vortices form in the wake of the sphere. For Reynolds numbers in the range of 100-200 instabilities in flow break up vortices. This phenomenon is called vortex shedding. (K. S. Raju, 2001)

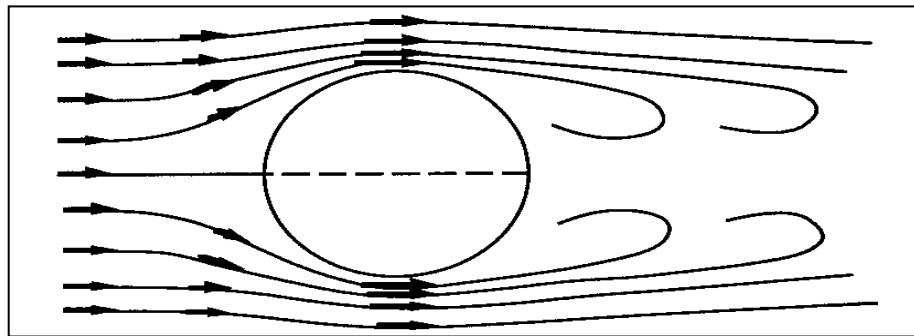


**Figure 2.7:** Vortex shedding in flow over a cylindrical body

Source: A. Cengal, (2006)

## 2.11 SIDE VIEW MIRROR

The automobile side-view mirror is a device for indirect vision that facilitates observance the traffic area adjacent to the vehicle which cannot be observed by direct vision. Being able to see what is behind the car is vital when reversing or changing lanes. The mirrors are often situated on, just in front of, the driver's and front passenger's doors. Due to legislation, today's cars have two mirrors. There are many regulations and laws when it comes to mirrors, mainly due to safety factors. Today's mirrors are made up of more than a reflective glass. The mirror housing often holds the indicators, illumination features and a blind spot alarm. The side view mirror (SVM) is a bluff body exposed to a high speed flow. The flow structure in the wake of the SVM is highly transient and will generate strong pressure fluctuation on the door panels and windows. This unsteady pressure fluctuation ultimately propagates into the carriage and exterior as noise (Olsson, 2002)

### 2.11.1 Designs

Mirrors have gone through many changes when it comes to appearance. In figure 2.8 designs over the years are shown. Often the esthetic design is more important than a good aerodynamic design. As time progresses aerodynamic aspects have become more important and influential. (Olsson, 2002)

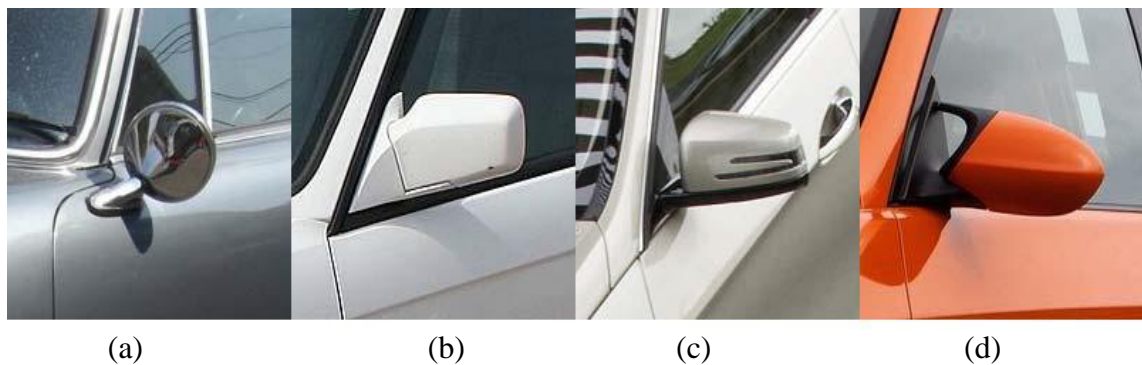


**Figure 2.8:** Different frontal area mirror designs over the years. (a) Is a Porsche 911T from 1972, (b) is a BMW M3 (E30) from 1988, (c) is a Mercedes-Benz E-class (W212) from 2010 and (d) is a BMW M3 GTS (E92) from 2011.

Source: Netcarshow.com, Asian-winds.com and Carbodykits.com (Olsson, 2002)

## **CHAPTER 3**

### **METHODOLOGY**

#### **3.1 INTRODUCTION**

The objective of this project can be achieved by preparing an organized methodology. This will make sure the project is capable to be completed on time. This chapter will explain the details about the methodology progress during Final Year Project 1 and 2. This chapter will list all the methods that were included and relevant to complete this project. The title “Computational Fluid Flow Analysis of a Side Mirror for a Passenger Car” was given by the faculty at the beginning of the semester. The literature study that is related to this topic has been carried out in Chapter 2.

The project will analyze the effect of side mirror on the car based on the pressure, velocity and drag using Computational Fluid Dynamic (CFD). ANSYS Fluent will be used to analyze the drag coefficient reduction by side mirror. This software will make the objectives to be achieved successfully. To solve all the problem, first thing to do is to determine all the flow works with the duration of time, the Gantt chart and flow chart is a recommended method to use. It is important so that all the flows work with the description of task carried out to meet the date line.

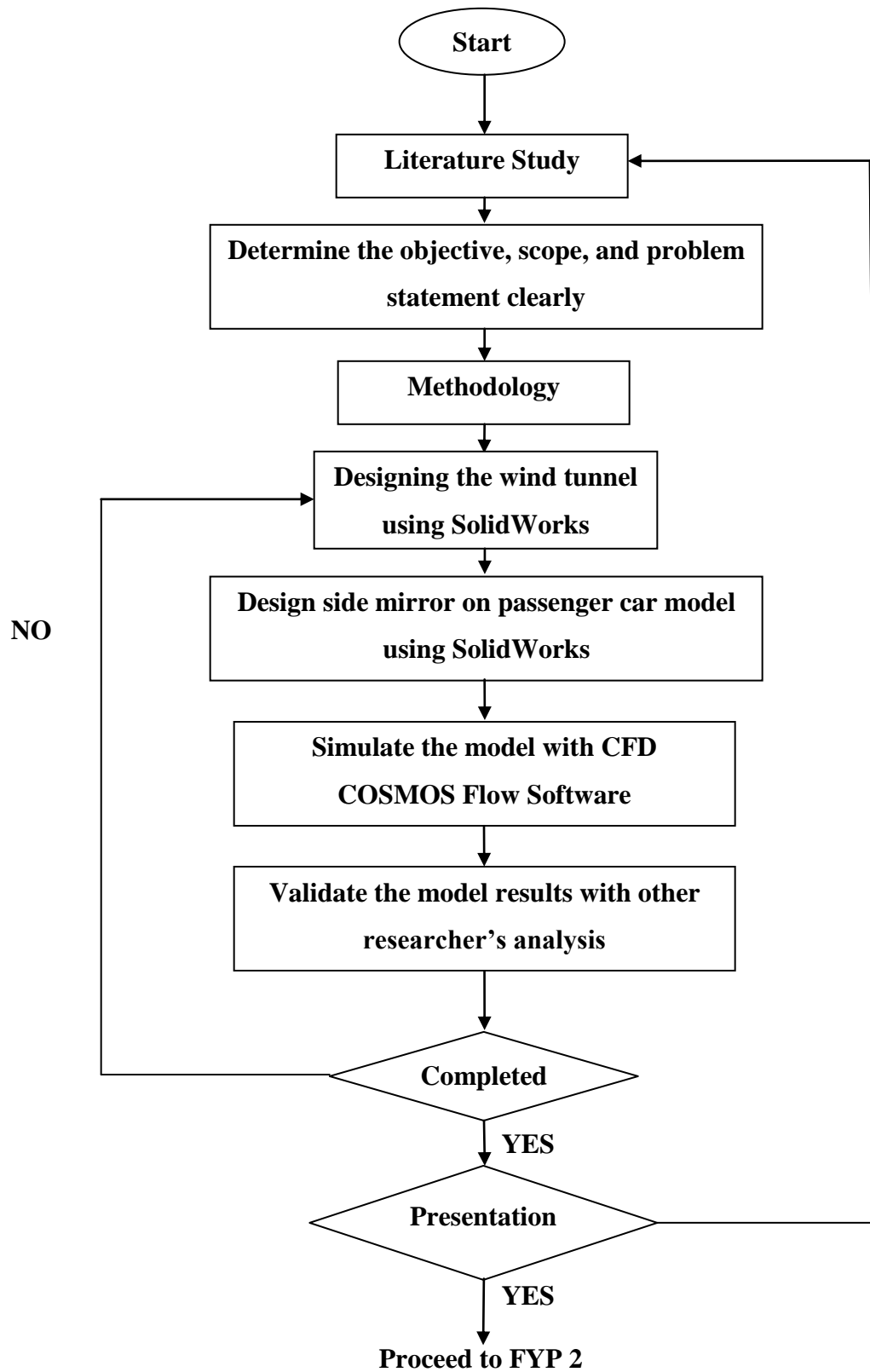


**Figure 3.1:** Methodology flow chart during FYP 1

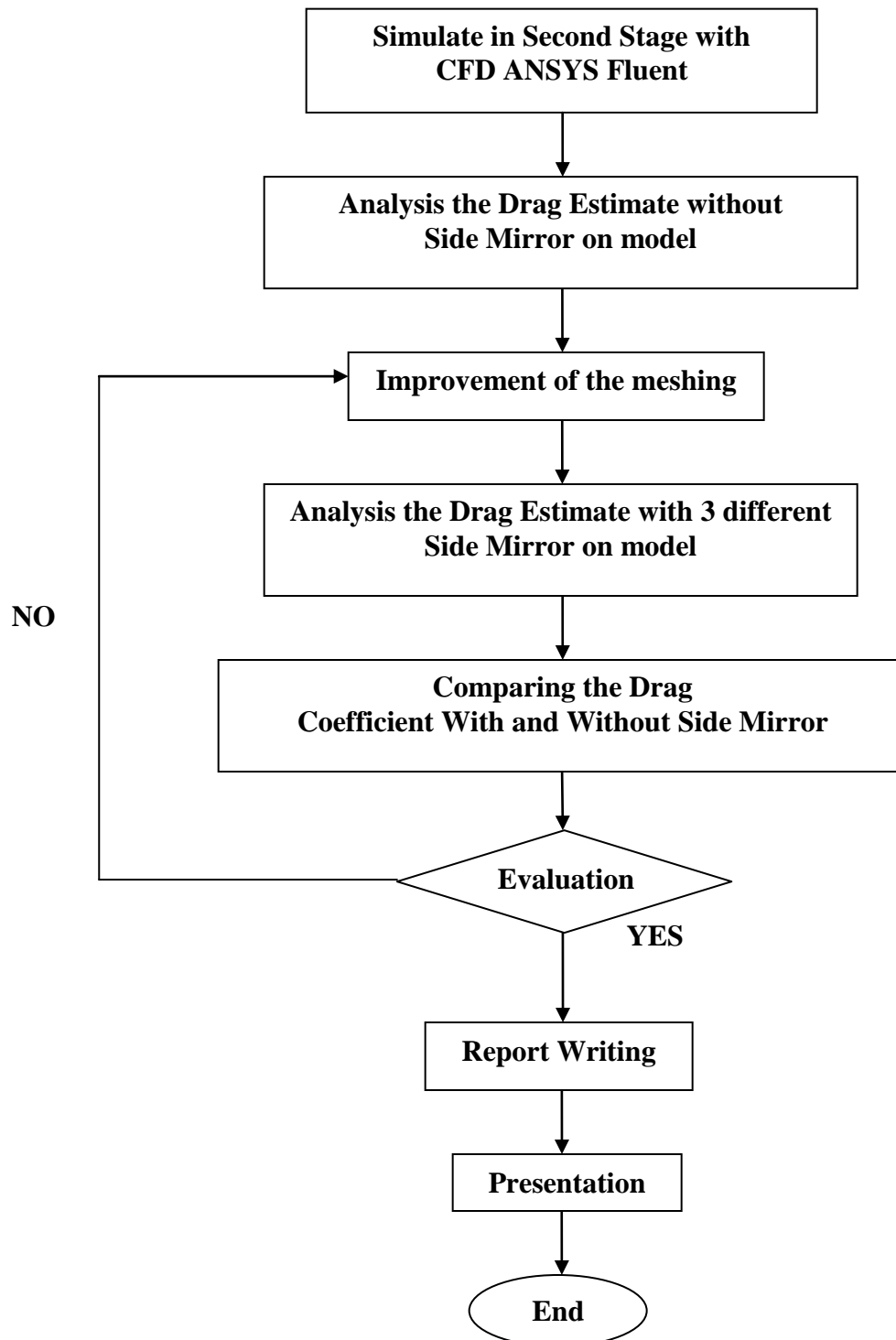


**Figure 3.2:** Methodology flow chart during FYP 2

## **3.2 FLOW CHART DESCRIPTION**

### **3.2.1 Project Introduction**

The project started with the title confirmation by the faculty. Upon discussion with the supervisor of the project, the main contents were determined. Project objective's is the most important part in this project. By the determination of the objective, the project will clearly see what will be doing from the beginning. The problem that will occur at the rear end of the car must be analyzed. This is very important so that the target objective from the starting can be achieved. The scopes of this project can be done after determine the objective. This will help the project to progress smoothly and can be success.

### **3.2.2 Literature Study**

This project is continued with literature review and research from the internet, company websites, books and journals about the title. This stage is very important while making literature review because the basic of the aerodynamics such as the flow characteristic around the vehicles , drag coefficient, lift coefficient , pressure distribution and others fluid dynamics requirement must be study. In this part, the detail about the design of the side mirror and all the effect about the external flow of the passenger car model will be explained. The literature study was added from the beginning of this project so that all the latest information will be updated from the time to time.

### **3.2.3 Problem Solving**

By referring to this project, the main problem solving is by using the Computational Fluid Dynamics Software to analyze the flow velocity and pressure distribution around the car body, to complete that, there must be a problem solving method or flow to complete. So, the works which involve in solving this problem must be organized. With referring to the methodology flow chart, the detail for each activity can be referring to next sub topics.

This part also can give the individual to understand what the important things needed before proceeding to the next stage.

### 3.3 COMPUTER AIDED DRAWINGS (CAD)

#### 3.3.1 Designing of Wind Tunnel

The greatest benefit from computational fluid dynamics is to gain insight into a particular phenomenon by establishing the trends in the aerodynamic characteristics. It is valuable in understanding and exploiting the trends of shape change that will affect the flow field and improve the aerodynamic of the model. However, before the CFD model with add on devise can be designed and simulated, CFD method for flow over passenger car needs to be validated against CFD simulation of flow over the same generic model. Based on the design of virtual wind tunnel by Yang and Khalighi in 2010, the wind tunnel has a length of 12m a height of 6m and width of 4m. Figure below shows the virtual wind tunnel to be used in this experiment.

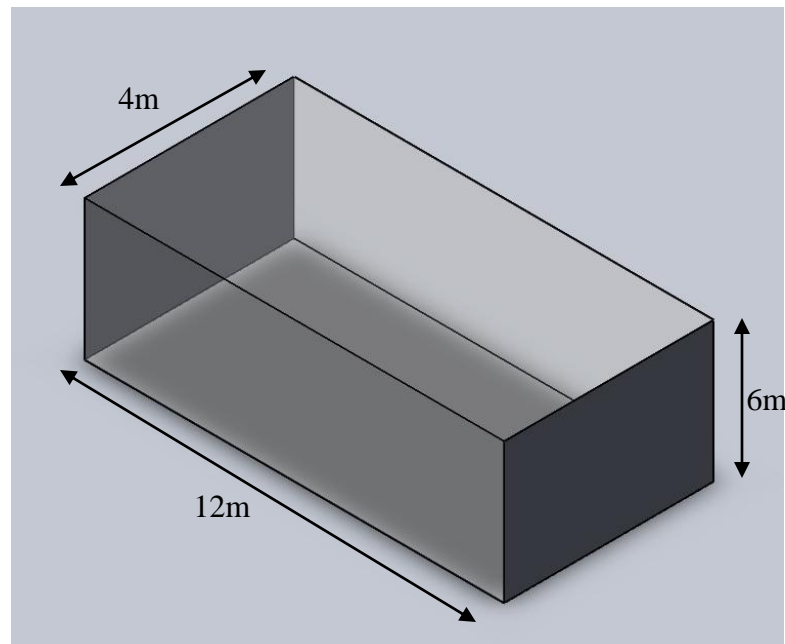


**Figure 3.3:** Virtual Wind Tunnel Design



### 3.3.2 Designing of Passenger Car

The generic model of the passenger car is shown in the Figure 3.4 and Figure 3.5 below with relevant dimensions. The model is using the actual dimension of car which the length of the model is 4.257m, the width of the model is 1.680m, and the height of the model is 1.502m. SolidWorks is used to produce the vehicle model with the required dimensions

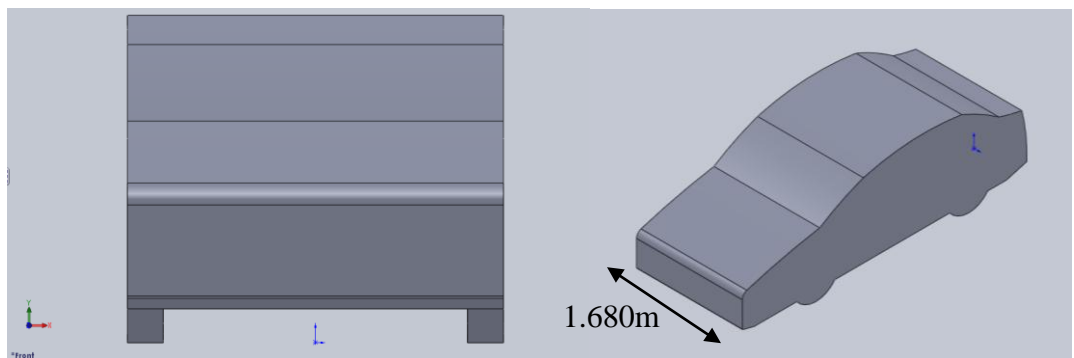


**Figure 3.4:** Front View and Isometric View of Passenger Car Model

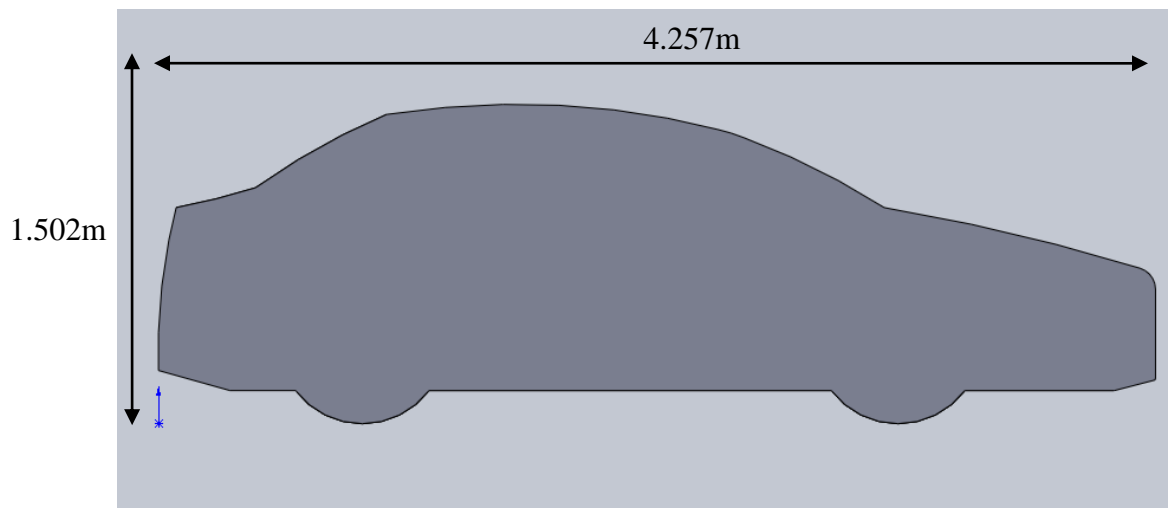


**Figure 3.5:** Side View of Passenger Car Model

### 3.3.3 Designing of Side Mirrors

The generic model of the side mirrors is shown in the Figure 3.6 to Figure 3.8 below with common dimensions. The model is using the actual common dimension of side mirror which is the length of the model is 1.310m, the width of the model is 0.540m, and the height of the model is 0.930m. SolidWorks is used to produce the models with the required dimensions. Design 1 was done based on a semi-sphere shape while Design 3 was done based on a sharp end with triangular shape and the Design 3 was done by combining rectangular shape with triangular edges.

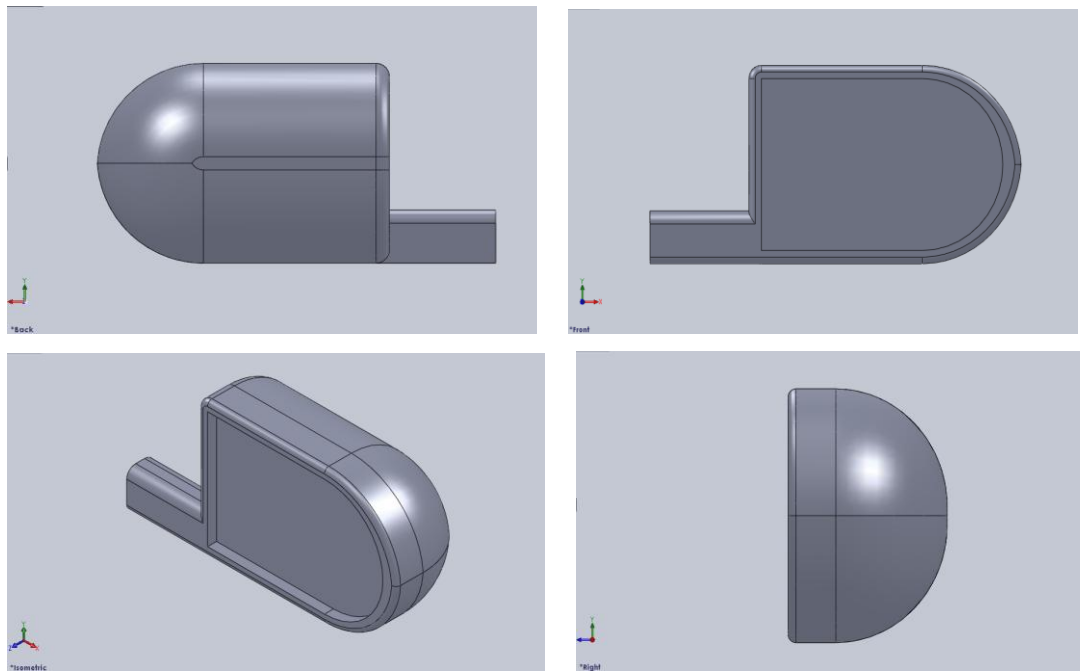


**Figure 3.6:** Design of Side Mirror 1

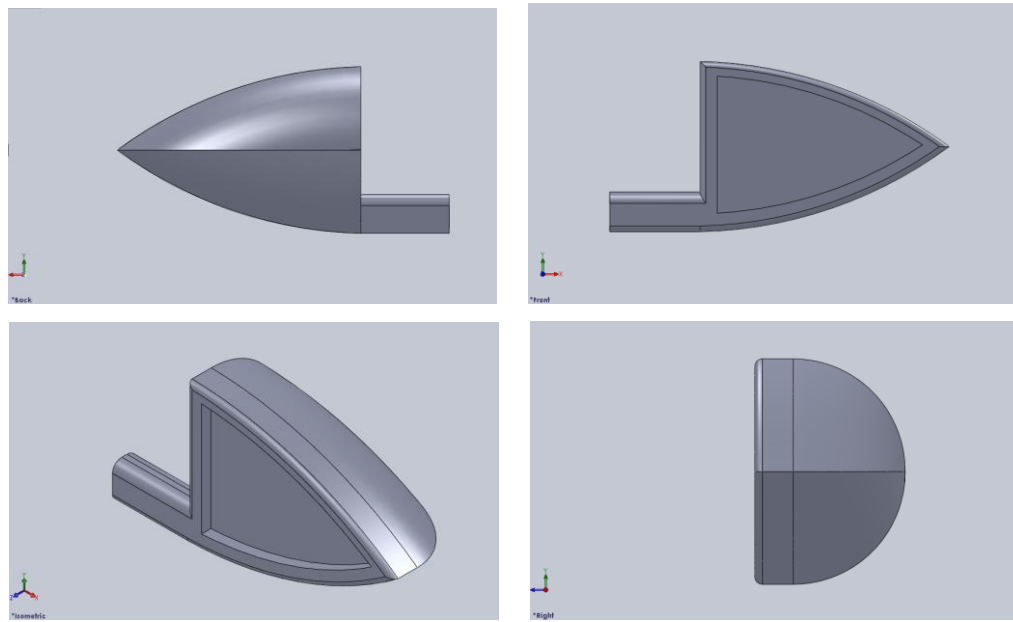


**Figure 3.7:** Design of Side Mirror 2

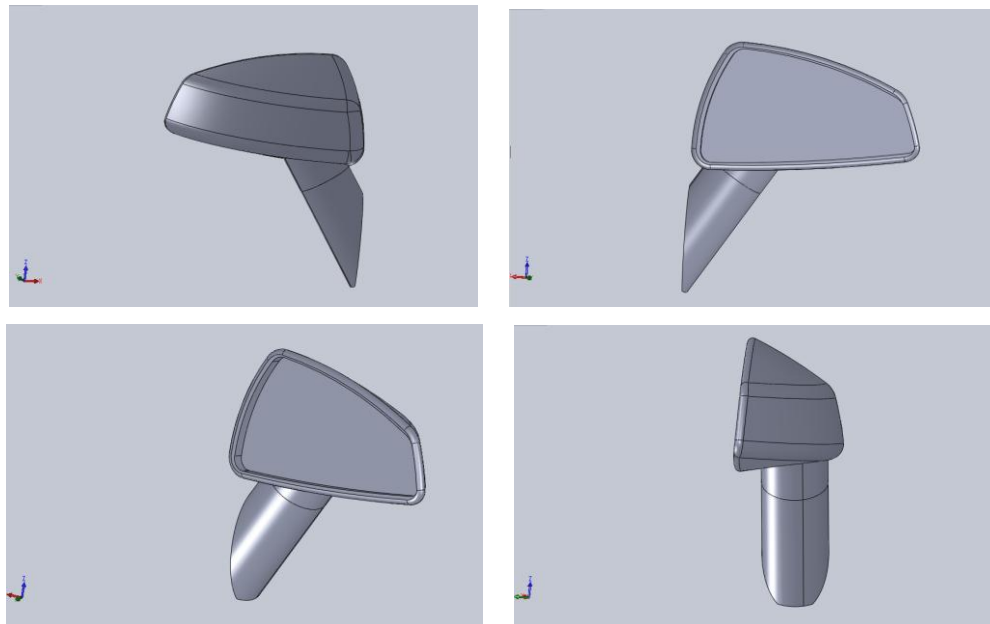


**Figure 3.8:** Design of Side Mirror 3

### 3.4 MESH GENERATION

Mesh generation is the practice of generating a polygonal or polyhedral mesh that approximates a geometric domain. Due to the simulation meshing characteristics, the method of triangulation was used in the wind tunnel simulation domains. Figure 3.9 shows the methods of triangulation used for the domain. The elements of triangular shape will be small when approaching the complex shape and small. Medium mesh was applied to simulate.

The virtual wind tunnel surface was discretized with a larger triangular mesh to define coarse meshes near the surface of the wind tunnel surface away from the passenger car model. After the surface meshes on the vehicle, three layers of prismatic layers were defined under the body surface of the vehicle.

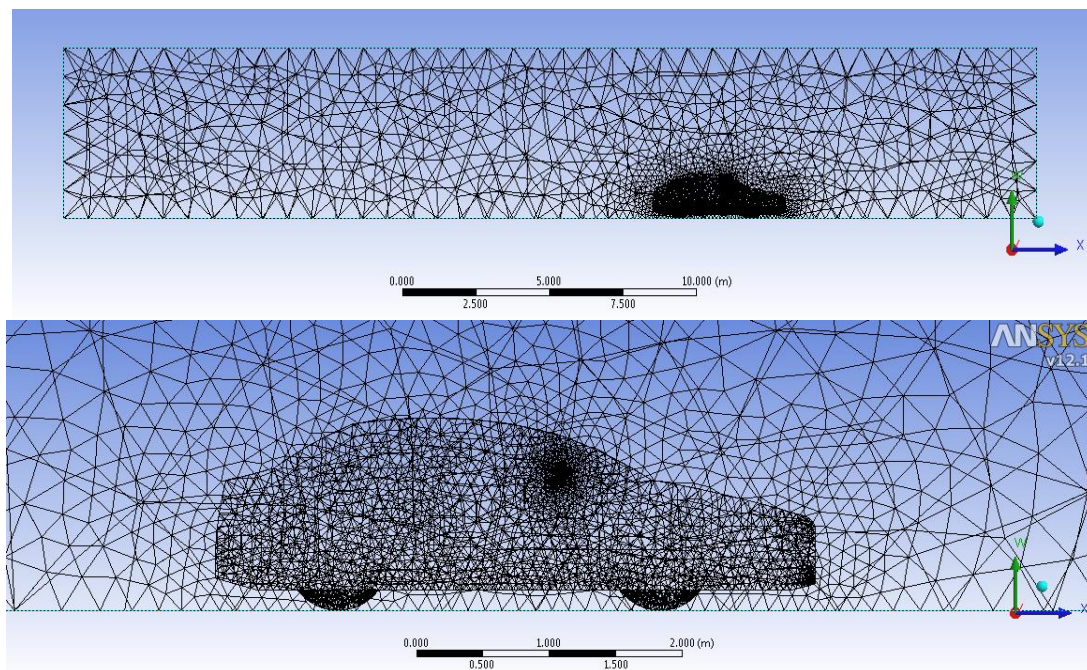


**Figure 3.9:** Meshing of wind tunnel and model

### 3.5 SIMULATION MODEL

The first component of the model car is created by using Design Modular in CFD by importing the geometry model to FLUENT program, which was placed inside the wind tunnel for testing flow simulation. Before that, the model is frozen to make a cavity model before creating the wind tunnel. The characteristics of the wind tunnel are as Figure 3.3.

The wind tunnel is considered is made up of a straight floor and roof with an inlet up stream of the car 8.145m distance ahead of the front of the car and the outlet 20m downstream of the car. So that, as the tunnel outlet is far from the car, it can be assumed that it will have a little effect on the air flow close to the car. The tunnel height is taken a 5m. Then the boundaries if the simulation model is the car surface, front grille, velocity inlet, pressure outlet, symmetry, symmetry upper, symmetry side and road.

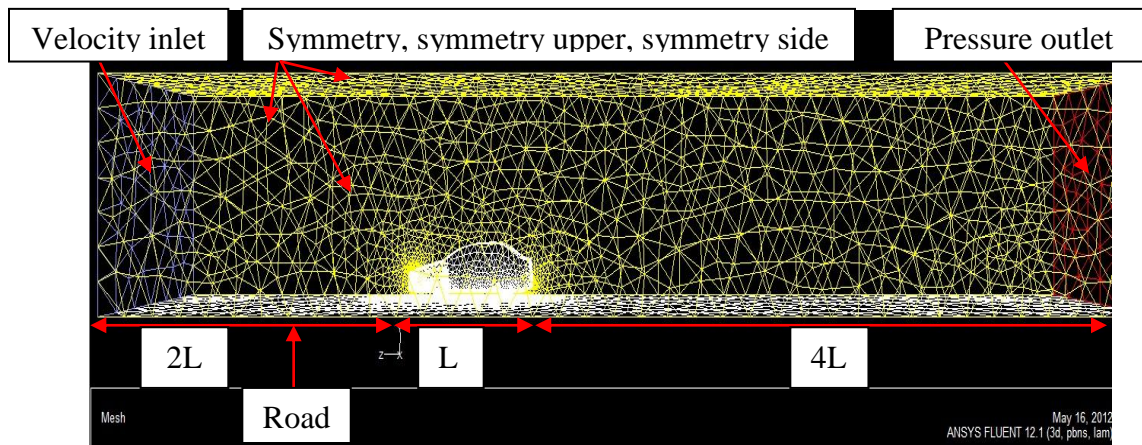


**Figure 3.10:** Wind Tunnel Boundary Setting

### 3.6 ASSUMPTIONS MADE

The assumptions made in present simulation were the air flow was steady state with constant velocity at inlet and with zero degree yaw angle, constant pressure outlet, no slip wall boundary conditions at the vehicle surfaces, and inviscid flow wall boundary condition on the top, sidewalls and ground face of the virtual wind tunnel.

### 3.7 SOLVER SETTING

The setting of passenger car numerical analysis requires being complete for the simulations. The solver setting includes type of solver (3D or 2D), the viscous model, boundary condition and solution controls. For this simulation, the 2D solver was chosen to analyze the form of air flow through the front grill. The inlet of the wind tunnel was carried out for different inlet air flow speed of 60 km/h and 180 km/h respectively. The outlet boundary was considered as 101.3 kPa (normal atmospheric pressure). The setting is as the following Table 3.1 and 3.2.

**Table 3.1:** Solver settings

<b>Turbulence Model</b>	k- $\epsilon$ (2 eqn)
<b>k-epsilon Model</b>	Standard
<b>Near-Wall Treatment</b>	Enhanced wall Function
<b>Operating Conditions</b>	Ambient

**Table 3.2:** Boundary Condition settings.

<b>Boundary Conditions</b>		
<b>Velocity Inlet</b>	<b>Magnitude (Measured normal to Boundary)</b>	16.67, 25 and 33.33 m/s (constant)
	<b>Turbulence Specification Method</b>	Intensity and Viscosity Ratio
	<b>Turbulence Intensity</b>	5.00%
	<b>Turbulence Viscosity Ratio</b>	10.00%
<b>Pressure Outlet</b>	<b>Gauge Pressure magnitude</b>	0 Pascal
	<b>Gauge Pressure direction</b>	Normal to boundary
	<b>Turbulence Specification Method</b>	Intensity and Viscosity Ratio
	<b>Backflow Turbulence Intensity</b>	1%
	<b>Backflow Turbulent Viscosity Ratio</b>	10%
<b>Wall Zones</b>	- Vehicle surface-non slip wall - Ground face- inviscid wall - Side faces -inviscid wall	
<b>Fluid Properties</b>	<b>Fluid Type</b>	Air
	<b>Density</b>	$\rho = 1.175 \text{ (kg/m}^3 \text{)}$
	<b>Kinematic viscosity</b>	$\nu = 1.7894 \times 10^{-5} \text{ (kg/(m}\cdot\text{s))}$

## **CHAPTER 4**

### **RESULTS AND DISCUSSION**

#### **4.1 INTRODUCTION**

The main objective of this project is to study the effects of flow in different velocities towards a side mirror of a passenger car. The experimented effect will be simulated using ANSYS FLUENT CFD software. Different types of side mirror models with different speeds will be simulated on a passenger car model to study the drag coefficient, lift coefficient and pressure coefficient of the model.

Accessories attached on the body skin of a car cause the unfavorable aerodynamic penalty in order to obtain the rear sight view. The results will be compared with an experiment done by researchers. The assumption used in this simulation is neglecting any flow frictions, steady and incompressible flow and the same material is used.

#### **4.2 CRITICAL POINTS ACROSS THE SIDE MIRROR**

Figure 4.1 show the selection of 100 critical points across the side mirror for all the designs used. This is done to extract the results which are pressure coefficient, total pressure, drag coefficient and lift coefficient at the required area. The critical points are chosen across the frontal area of the side mirror which faces the simulated flow.



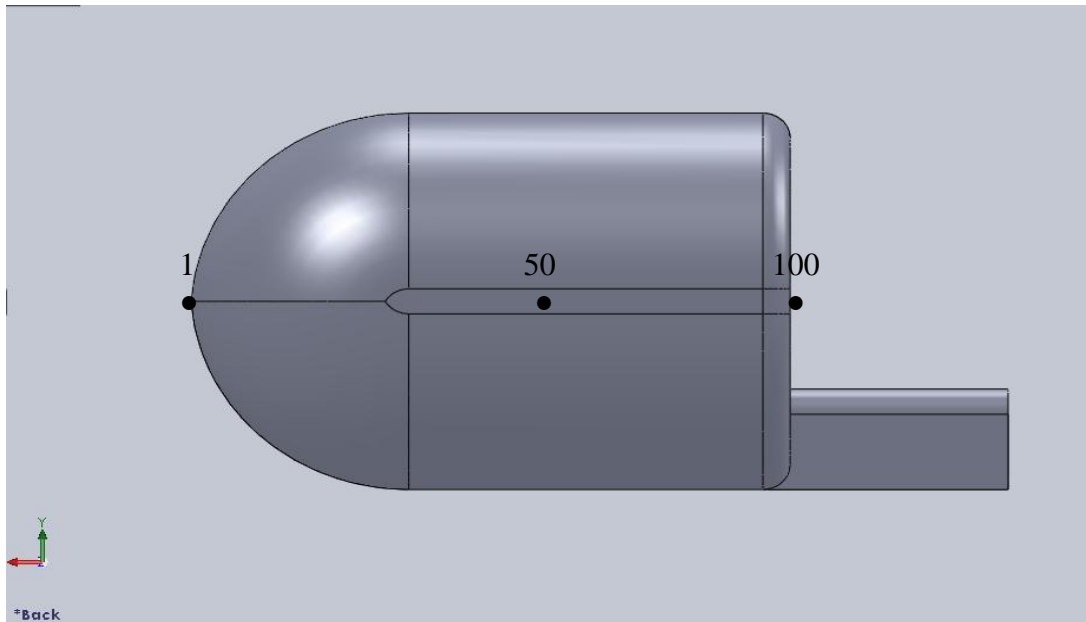


**Figure 4.1:** Example of side mirror with 100 critical points

### 4.3 PRESSURE COEFFICIENT, $C_p$

The pressure coefficient at a point near a body is independent with the body size. To determine the model, it is tested in a wind tunnel or water tunnel, pressure coefficients is determined at critical locations around the model and these pressure coefficients is used with confidence to predict the fluid pressure at those critical locations around a passenger car.

#### 4.3.1 Pressure Coefficient, $C_p$ for 16.67m/s (60km/h)

The pressure coefficient graph was produced and the value for pressure coefficient in different points on the side mirror 1 in 16.67m/s speed is shown in Figure 4.2. The contours in Figure 4.2 show that the pressure coefficient around the side mirror is low then the pressure distribution around the passenger car. There are circular patterns surrounding the side mirror which indicates the pressure difference around the side mirror. There are eddies forming at the back of the side mirror.

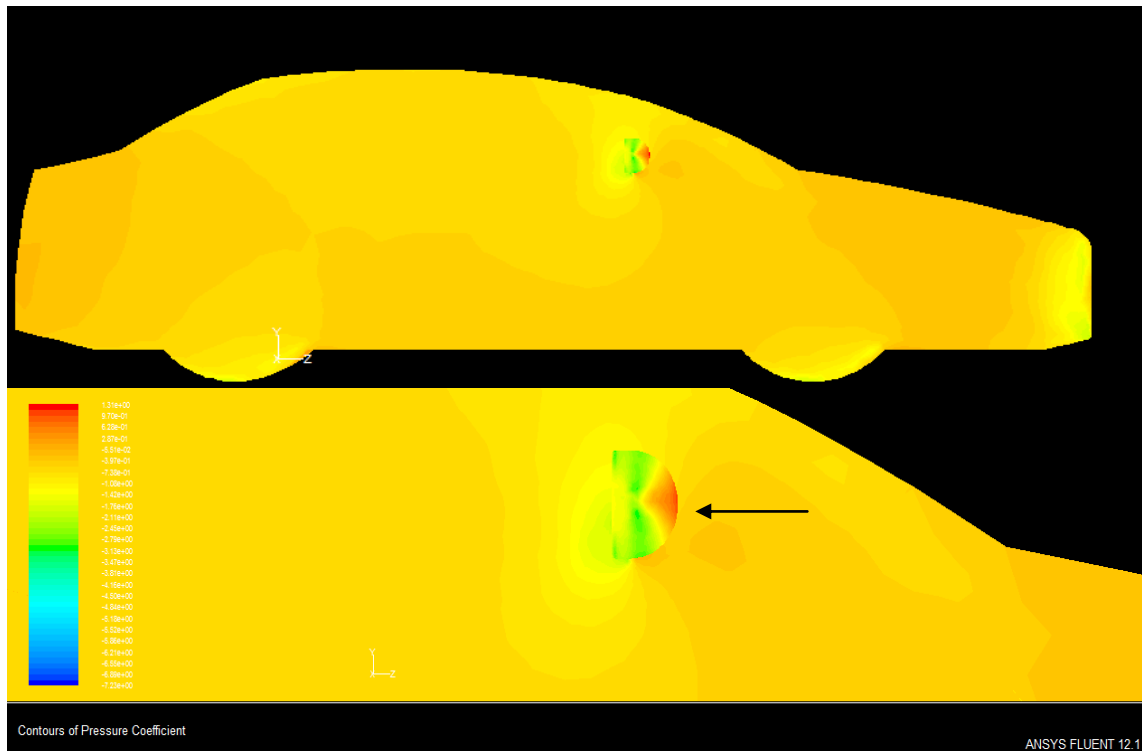


**Figure 4.2:** Pressure coefficient ( $C_p$ ) contour for Model 1 (16.67m/s)

Based on the graph in Figure 4.3, the data obtained from the simulation result shows that the pressure coefficient in point 73 to point 94 of side mirror 1 is extremely low (minimum point: -5.837) which is the gap area between the side mirror body and the car body. At point 0 to 73 the  $C_p$  is in average value of -1.5. That could be the optimum pressure coefficient for the speed of 16.67m/s of this model.

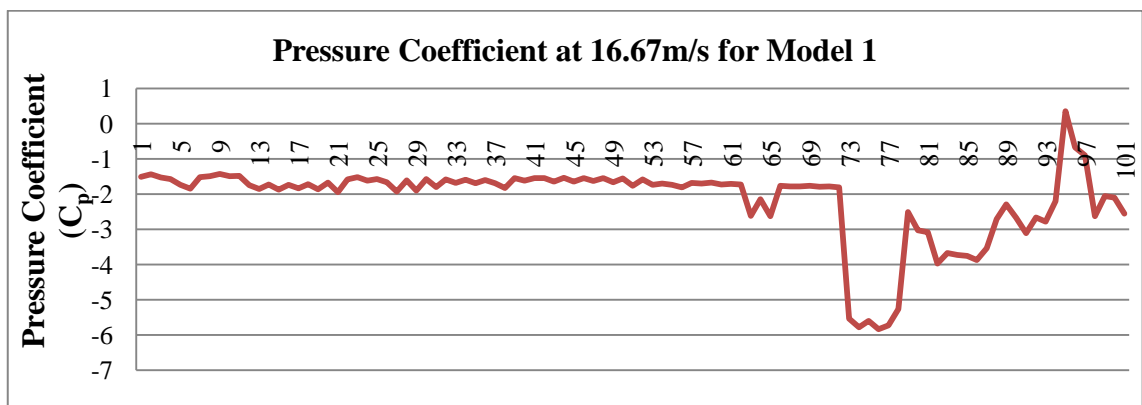


**Figure 4.3:** Graph of Pressure Coefficient of 100 critical points across Side Mirror 1 frontal area

The pressure coefficient graph is produced and the value for pressure coefficient in different points on the side mirror 2 in 16.67m/s speed is shown as in Figure 4.4. The contours below as shown in Figure 4.4 show that the pressure coefficient around the side mirror is low then the pressure distribution around the passenger car. There are circular pattern of pressure towards the upwards of the side mirror. There is small eddies forming at the back.

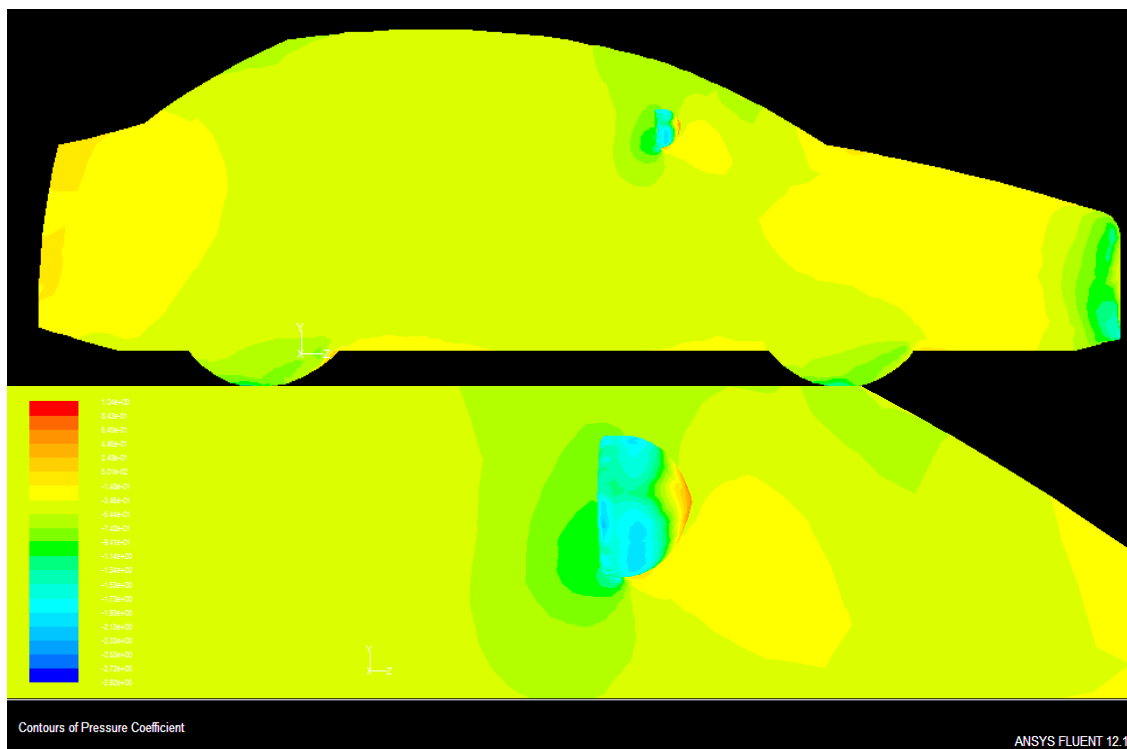


**Figure 4.4:** Pressure coefficient ( $C_p$ ) contour for Model 2 (16.67m/s)

Based on the graph in Figure 4.5, the data obtained from the simulation result shows that the pressure coefficient is much distorted. Point 28 and point 82 has the lowest pressure coefficient which is below -2.5. That area could be the starting point and end point of the curvature along the frontal area which is facing the flow. The average pressure coefficient is around -2 to -1.5 for this model.

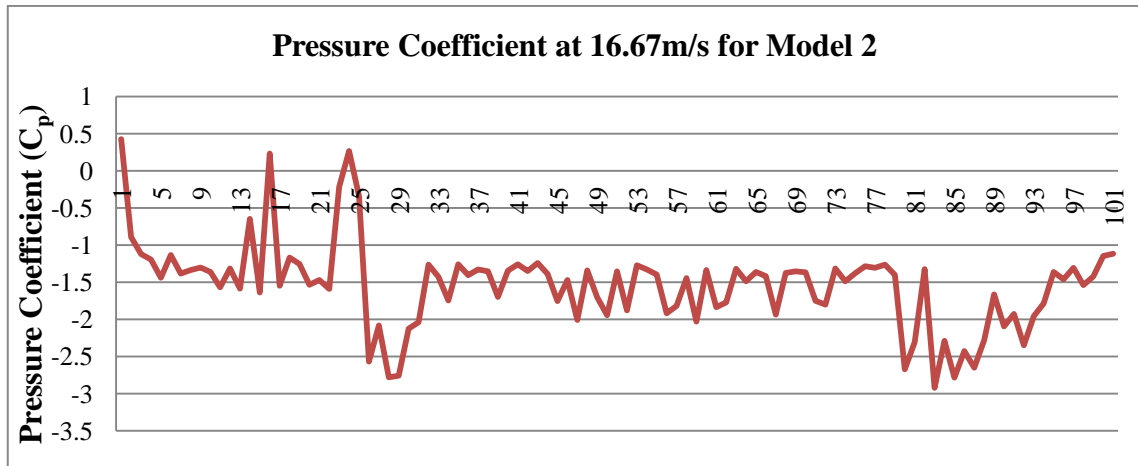


**Figure 4.5:** Graph of Pressure Coefficient of 100 critical points across side mirror 2 frontal area

The pressure coefficient graph is produced and the value for pressure coefficient in different points on the side mirror 3 in 16.67m/s speed is shown as in Figure 4.6. The contours below as shown in Figure 4.6 show that the pressure coefficient around the side mirror is low then the pressure distribution around the passenger car. There are circular pattern of pressure towards the downwards of the side mirror. There is higher eddies forming at the back.

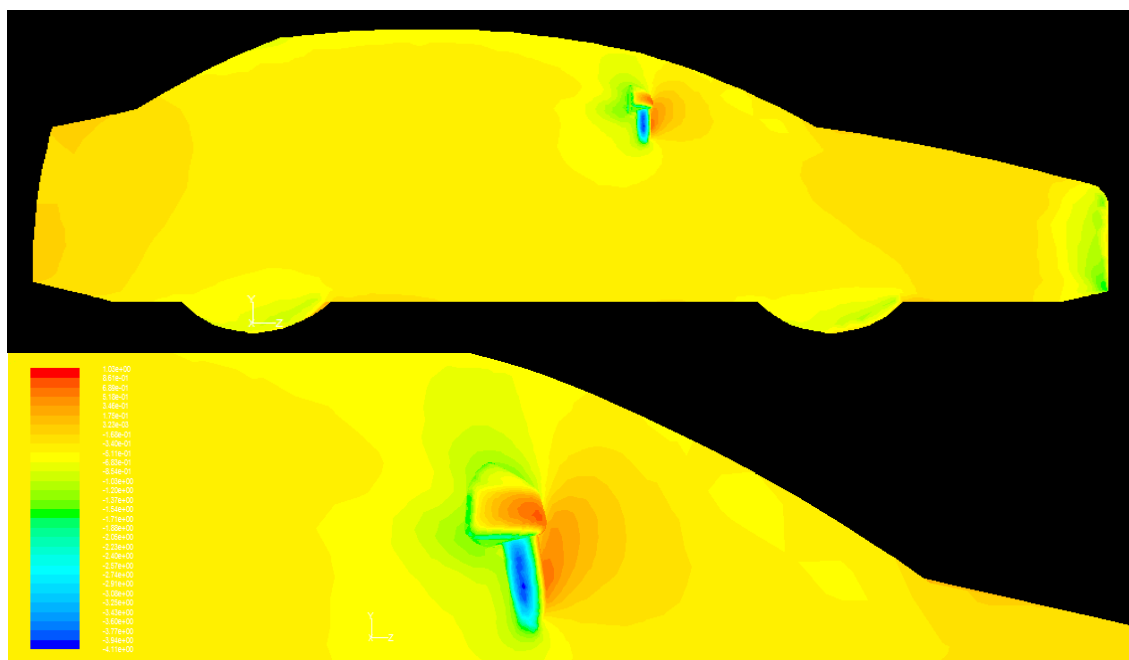


**Figure 4.6:** Pressure coefficient ( $C_p$ ) contour for Model 3 (16.67m/s)

Based on the graph in Figure 4.7, the data obtained from the simulation result shows that the pressure coefficient in point 21 to point 51 of side mirror 3 is extremely high which could be the flat surface at the back of the mirror. The average of the pressure coefficient for this speed is around -1 to -1.5. The fluxing pressure coefficient could cause noise and vibration to the side window.

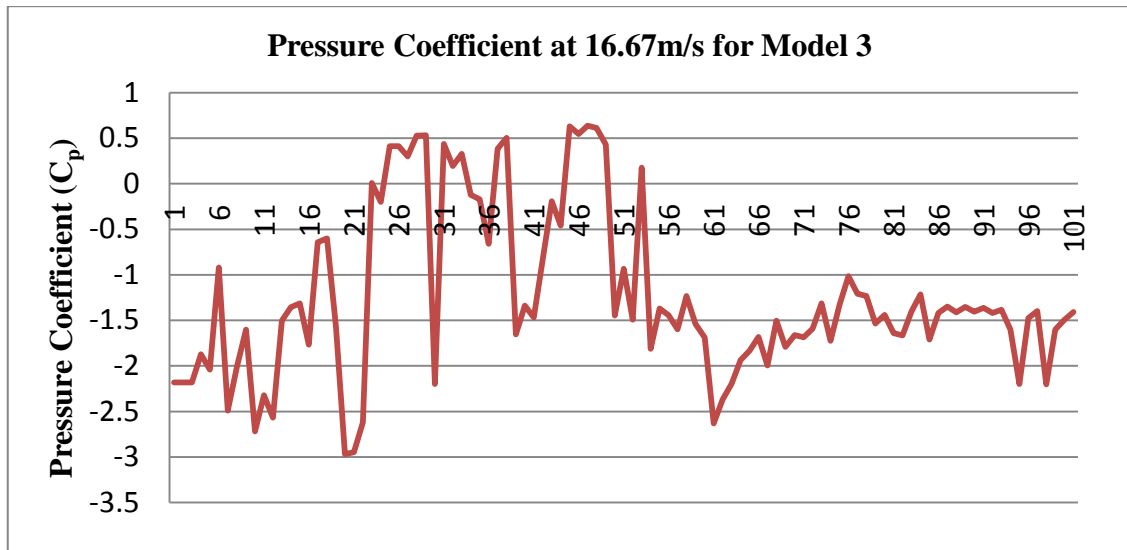


**Figure 4.7:** Graph of Pressure Coefficient of 100 critical points across side mirror 3 frontal area

#### 4.3.2 Pressure Coefficient, $C_p$ for 25m/s (90km/h)

The pressure coefficient graph is produced and the value for pressure coefficient in different points on the side mirror 1 in 25m/s speed is shown as in Figure 4.8. The contours below as shown in Figure 4.8 show that the pressure coefficient around the side mirror is low then the pressure distribution around the passenger car. There are circular pattern of pressure towards the upwards of the side mirror. There is small eddies forming at the back.

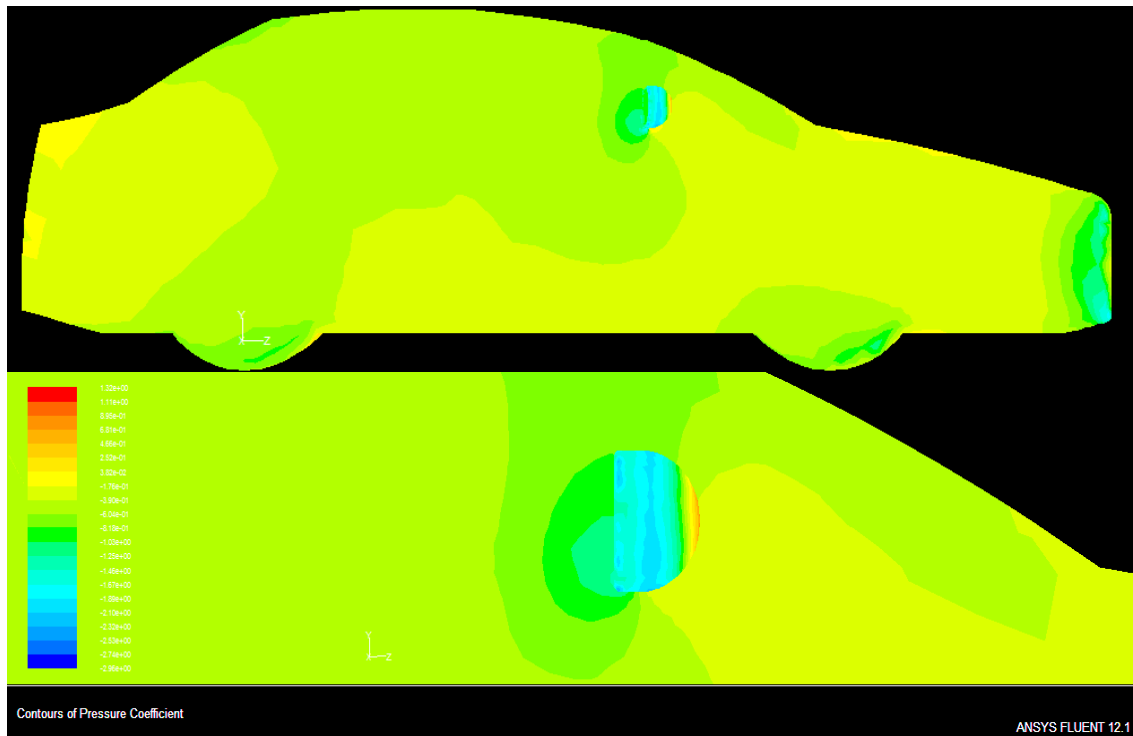


**Figure 4.8:** Pressure coefficient ( $C_p$ ) contour for Model 1 (25m/s)

Based on the graph in Figure 4.9, the data obtained from the simulation result shows that the pressure coefficient along the side mirror 1 is not fluctuating too much and is around the same region. The average pressure coefficient for this model in 25m/s speed is around -1 to -1.2 only. This means the side mirror design could have less noise and vibration.

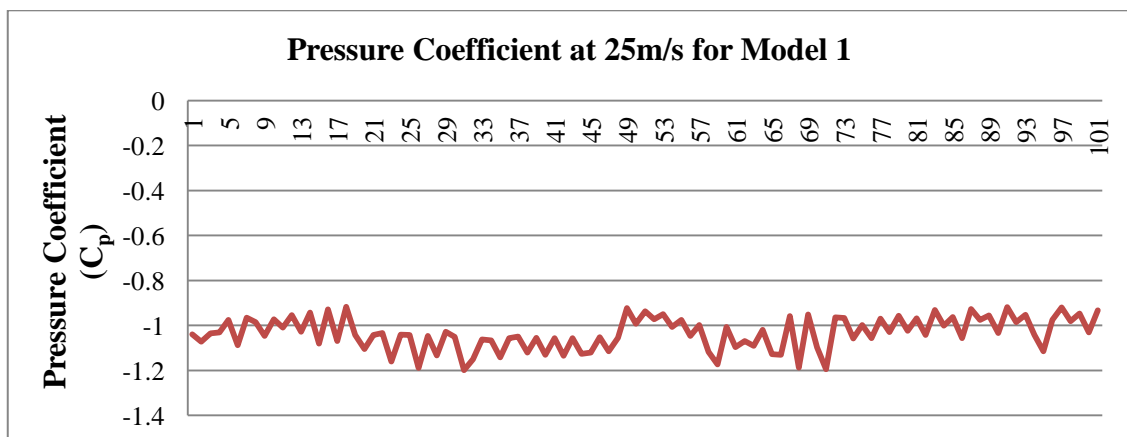


**Figure 4.9:** Graph of Pressure Coefficient of 100 critical points across side mirror 1 frontal area

The pressure coefficient graph is produced and the value for pressure coefficient in different points on the side mirror 2 in 25m/s speed is shown as below in Figure 4.10. The contours below as shown in Figure 4.10 show that the pressure coefficient around the side mirror is low then the pressure distribution around the passenger car. There are circular pattern of pressure towards the back of the side mirror. There is small eddies forming at the front of the mirror.

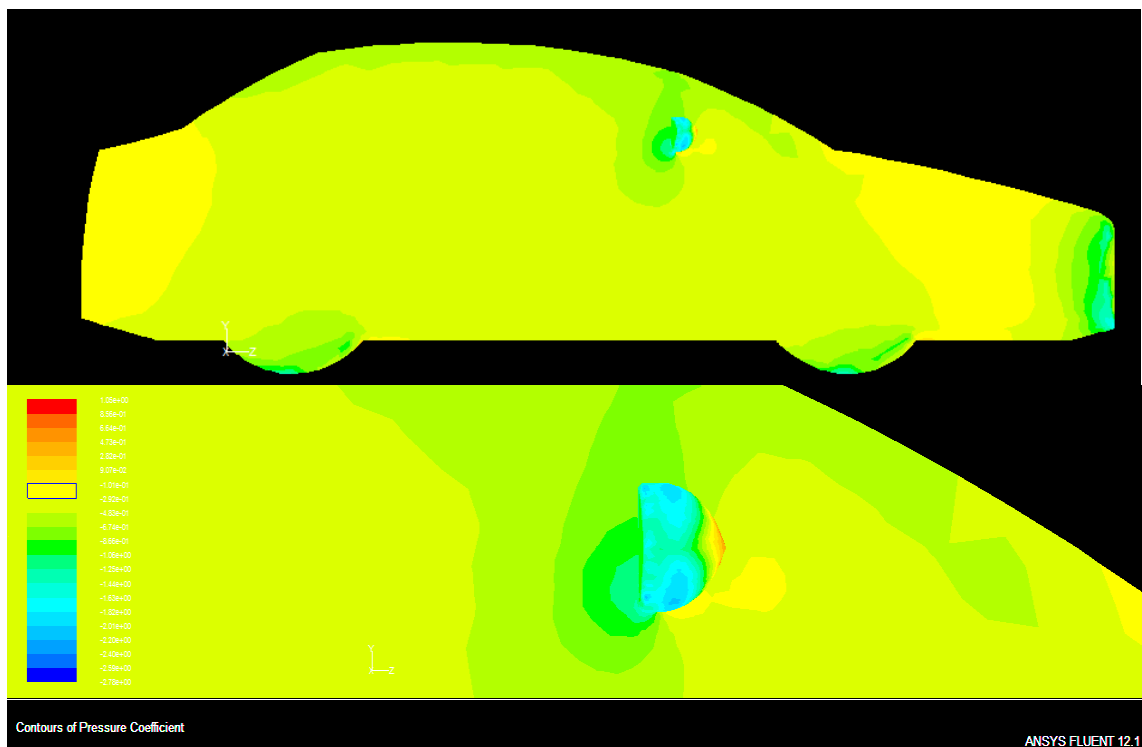


**Figure 4.10:** Pressure coefficient ( $C_p$ ) contour for Model 2 (25m/s)

Based on the graph in Figure 4.11, the data obtained from the simulation result shows that graph is very fluctuating. The pressure coefficient in point 28 to point 85 of side mirror 2 is extremely low (minimum point: -2.703) which is the sharp end at the back of the side mirror due to its curvature. At point 40 to 73 the  $C_p$  is in average value of -1.5. That could be the optimum pressure coefficient for the speed of 25m/s of this model.

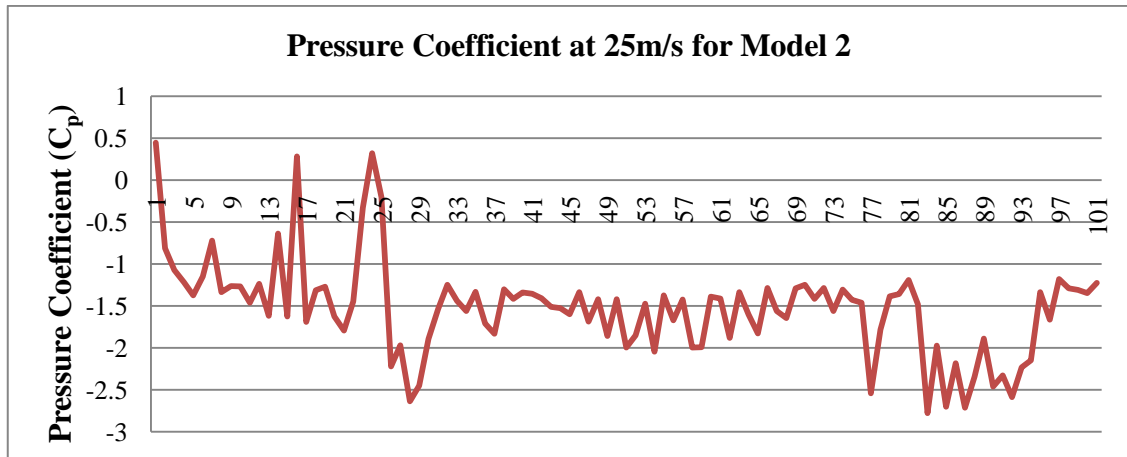


**Figure 4.11:** Graph of Pressure Coefficient of 100 critical points across side mirror 2 frontal area

The pressure coefficient graph is produced and the value for pressure coefficient in different points on the side mirror 3 in 25m/s speed is shown as in Figure 4.12. The contours below as shown in Figure 4.12 show that the pressure coefficient around the side mirror is low then the pressure distribution around the passenger car. There are circular pattern of pressure towards the front of the side mirror. There is small eddies forming at the front.

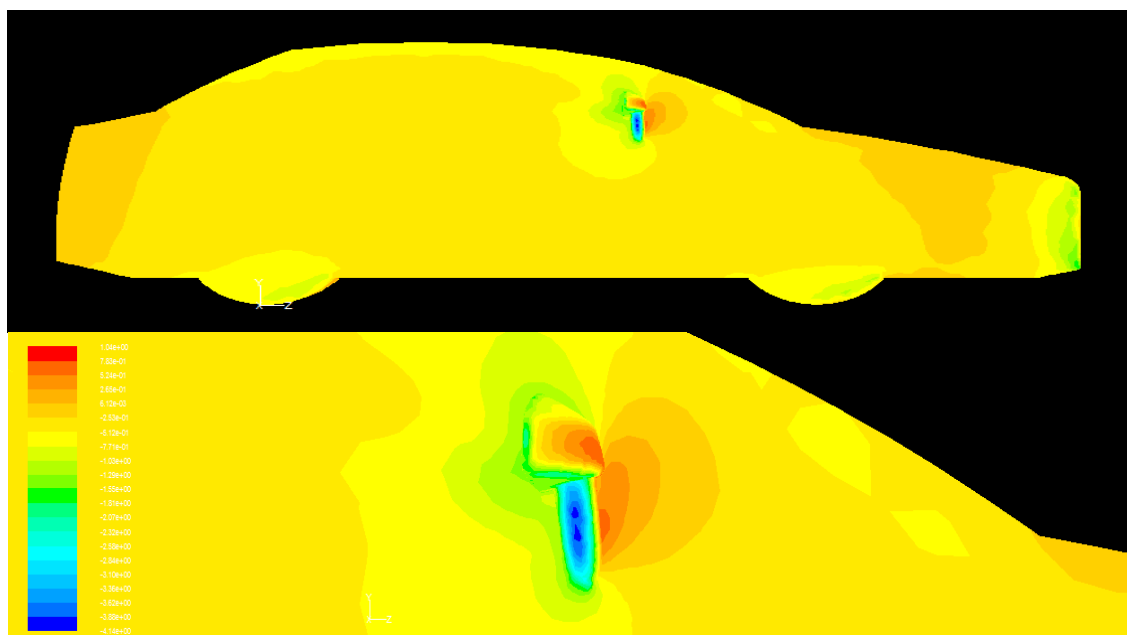


**Figure 4.12:** Pressure coefficient ( $C_p$ ) contour for Model 3 (25m/s)



Based on the graph in Figure 4.13, the data obtained from the simulation result shows that the pressure coefficient in point 22 to point 55 of side mirror 3 is extremely high (maximum point: 0.6128) which is side mirror holder and the car body. At point 61 to 94 the  $C_p$  is in average value of -1.54. That could be the optimum pressure coefficient for the speed of 25m/s of this model.

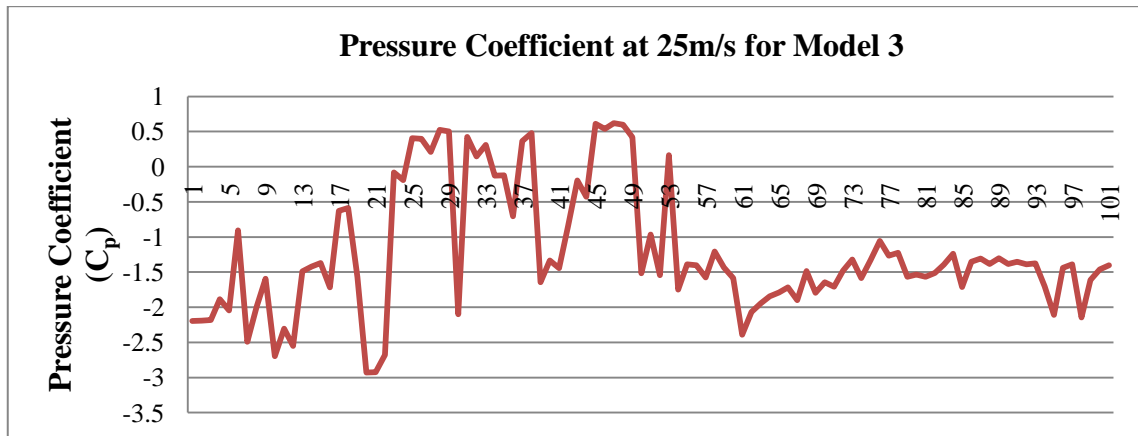


**Figure 4.13:** Graph of Pressure Coefficient of 100 critical points across side mirror 3 frontal area

#### 4.3.3 Pressure Coefficient, $C_p$ for 33.33m/s (120km/h)

The pressure coefficient graph is produced and the value for pressure coefficient in different points on the side mirror 1 in 33.33m/s speed is shown as below in Figure 4.14. The contours below as shown in Figure 4.14 show that the pressure coefficient around the side mirror is low then the pressure distribution around the passenger car. There are circular pattern of pressure towards the backwards of the side mirror. There is small eddies forming at the back.

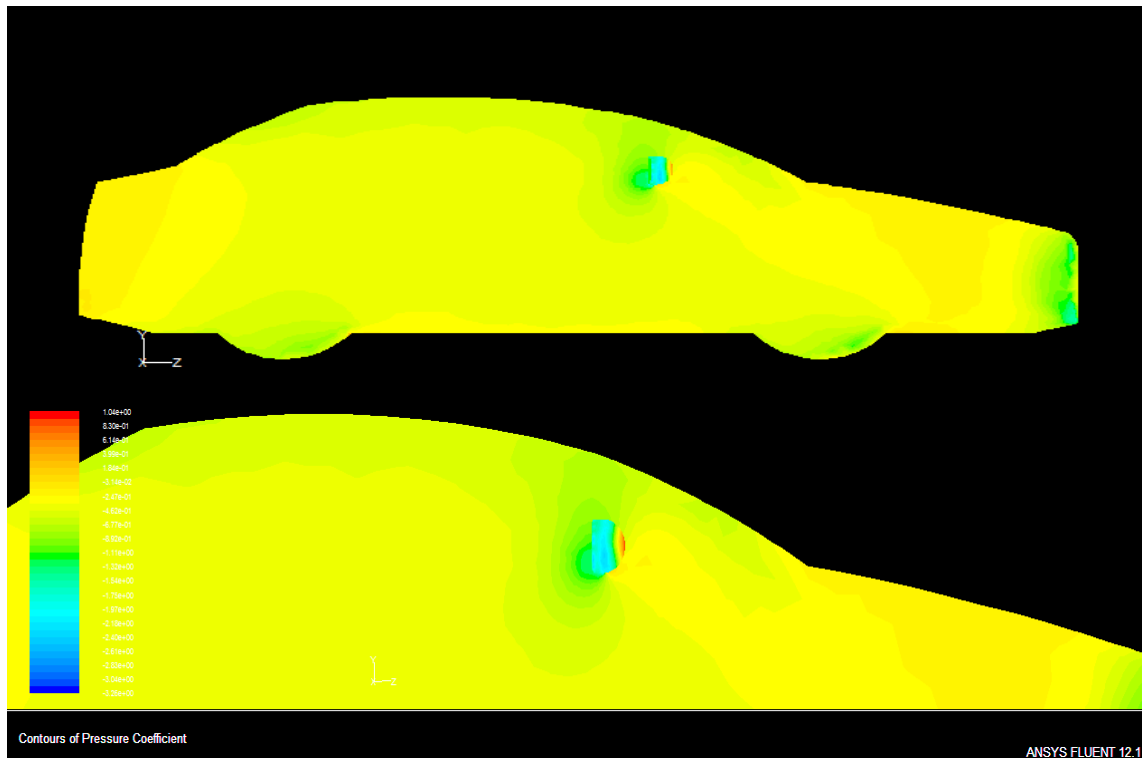


**Figure 4.14:** Pressure coefficient ( $C_p$ ) contour for Model 1 (33.33m/s)

Based on the graph in Figure 4.15, the data obtained from the simulation result shows that the pressure coefficient along the critical points is in average fluctuation which is around -1 to -1.5. This could happen because the curvature of the side mirror is asymmetrical to the flow direction. At point 22 to 49 the  $C_p$  is in average value of -1.1. That could be the optimum pressure coefficient for the speed of 33.33m/s of this model.

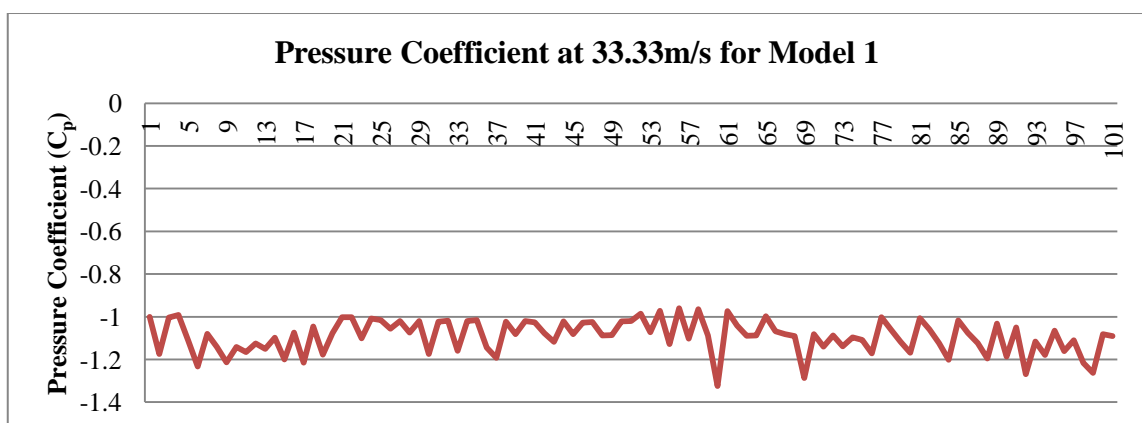


**Figure 4.15:** Graph of Pressure Coefficient of 100 critical points across side mirror 1 frontal area

The pressure coefficient graph is produced and the value for pressure coefficient in different points on the side mirror 2 in 33.33m/s speed is shown as below in Figure 4.16. The contours below as shown in Figure 4.16 show that the pressure coefficient around the side mirror is low then the pressure distribution around the passenger car. There are circular pattern of pressure towards the backwards of the side mirror. There is small eddies forming at the back.

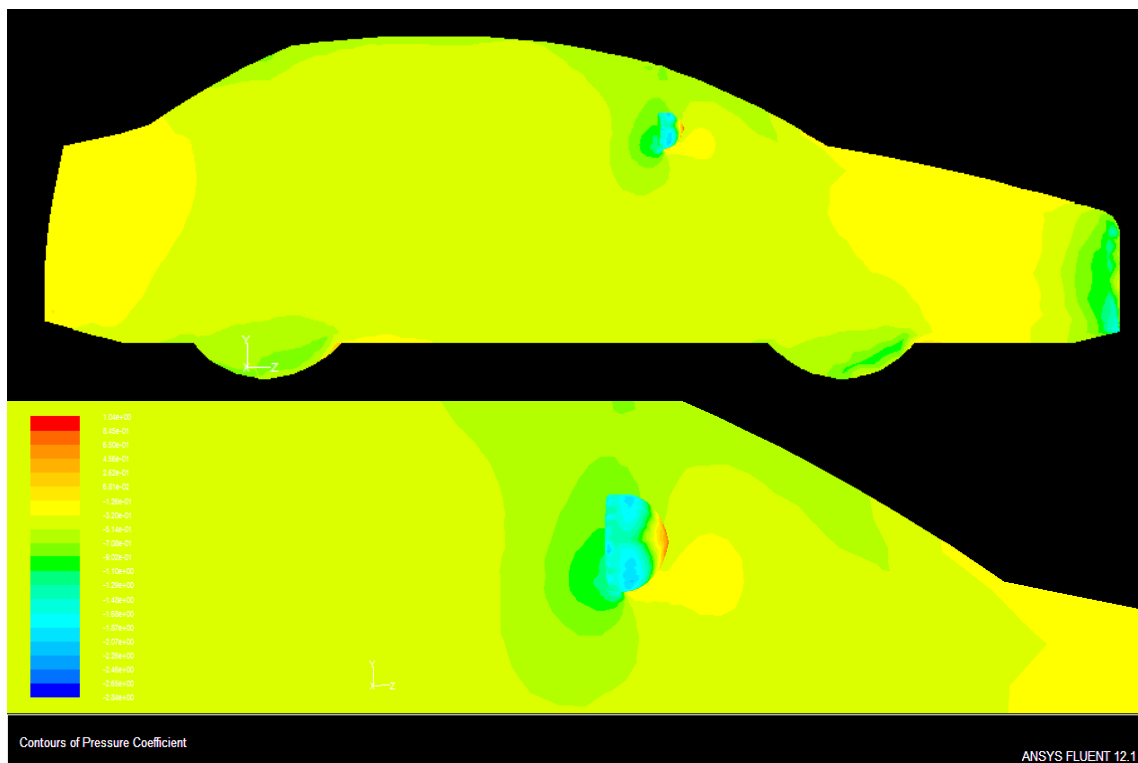


**Figure 4.16:** Pressure coefficient ( $C_p$ ) contour for Model 2 (33.33m/s)

Based on the graph in Figure 4.17, the data obtained from the simulation result shows that the pressure coefficient is very fluctuating between point 19-58 and 61-100. This could be happening because the side mirror could receive more pressure in high speed air flow which is 33.33m/s.

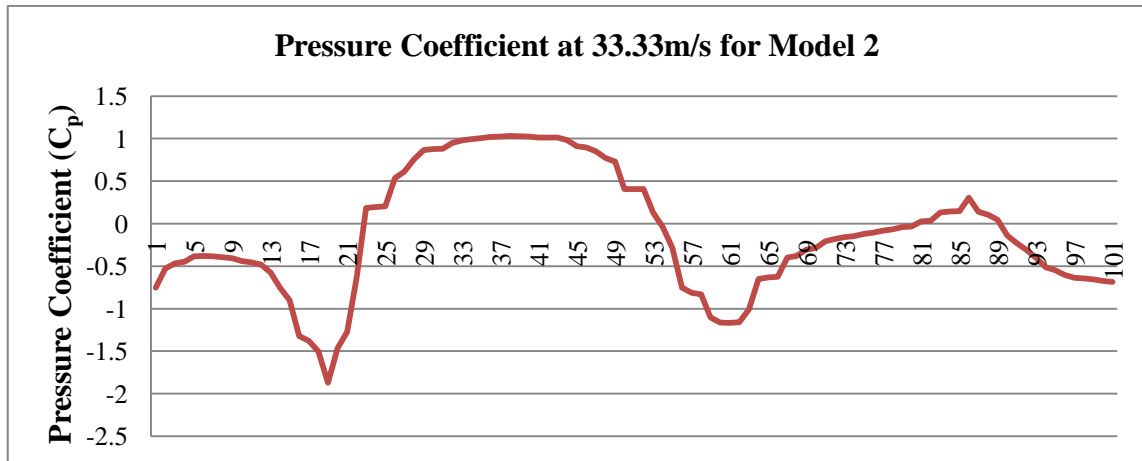


**Figure 4.17:** Graph of Pressure Coefficient of 100 critical points across side mirror 2 frontal area

The pressure coefficient graph is produced and the value for pressure coefficient in different points on the side mirror 3 in 33.33m/s speed is shown as below in Figure 4.18. The contours below as shown in Figure 4.18 show that the pressure coefficient around the side mirror is low then the pressure distribution around the passenger car. There are circular pattern of pressure towards the front of the side mirror. There is small eddies forming at the front.

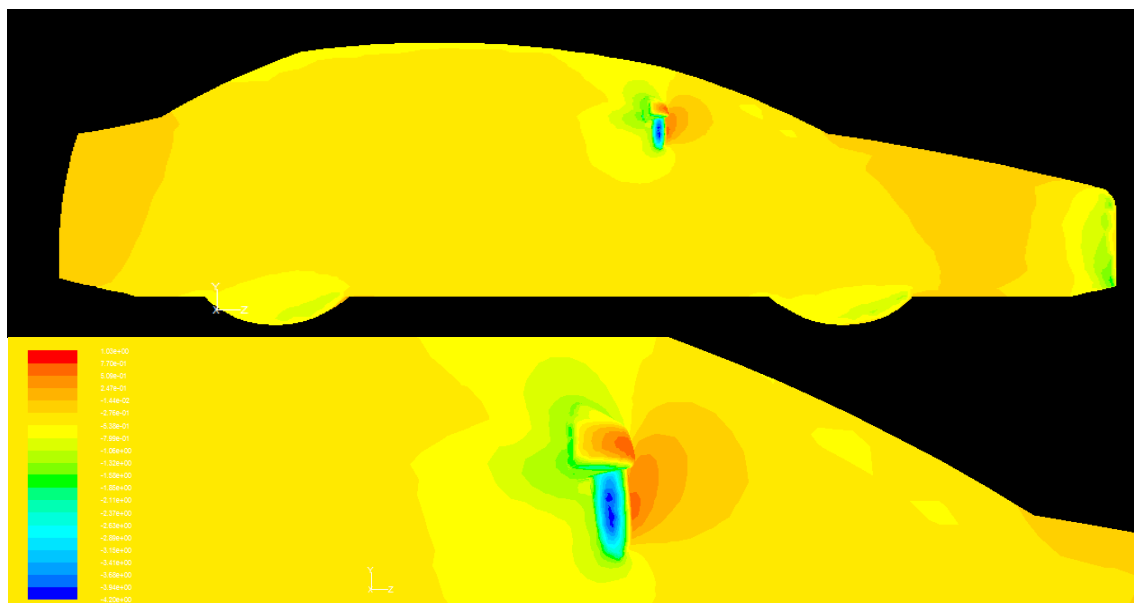


**Figure 4.18:** Pressure coefficient ( $C_p$ ) contour for Model 3 (33.33m/s)

Based on the graph in Figure 4.19, the data obtained from the simulation result shows that the pressure coefficient is highest in point 22 to 55 which is the frontal area of the side mirror. The highest pressure coefficient is in point 47 with a value of 0.622. That could be the optimum pressure coefficient for the speed of 33.33m/s of this model.

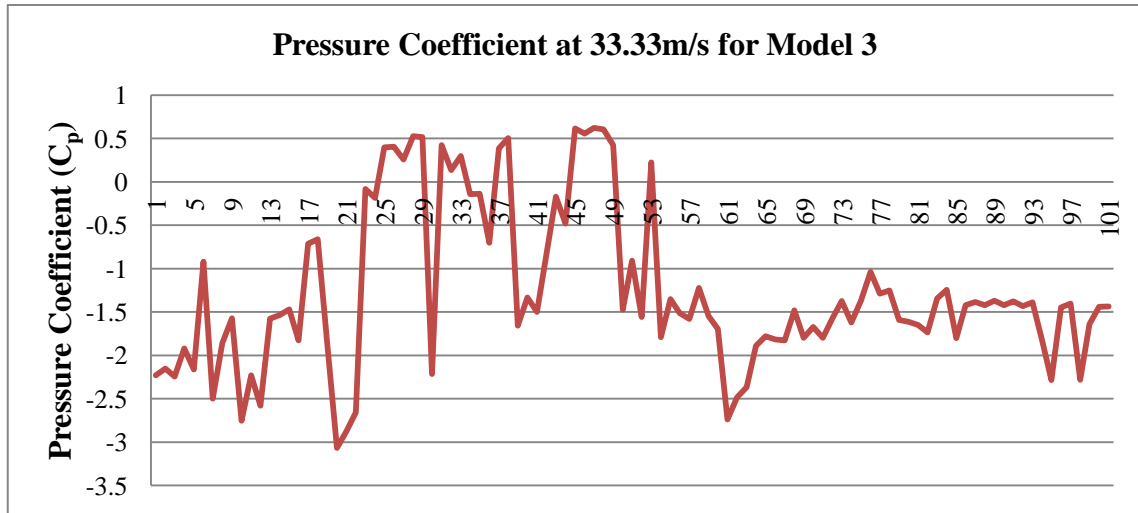


**Figure 4.19:** Graph of Pressure Coefficient of 100 critical points across side mirror 3 frontal area

#### 4.4 TOTAL PRESSURE, $P_{TOTAL}$

##### 4.4.1 Total Pressure, $P_{Total}$ for 16.67m/s (60km/h)

The Figure 4.20 shows the total pressure distribution along the side view of a passenger car using Model 1. Contour colors shows that the total pressure area which does not contact with the air flow is low while the frontal area of side mirror has high total pressure. This may be caused by the blunt shape of the side mirror. The pressure difference between the side mirror and passenger car body could cause noise and mirror fluctuations.

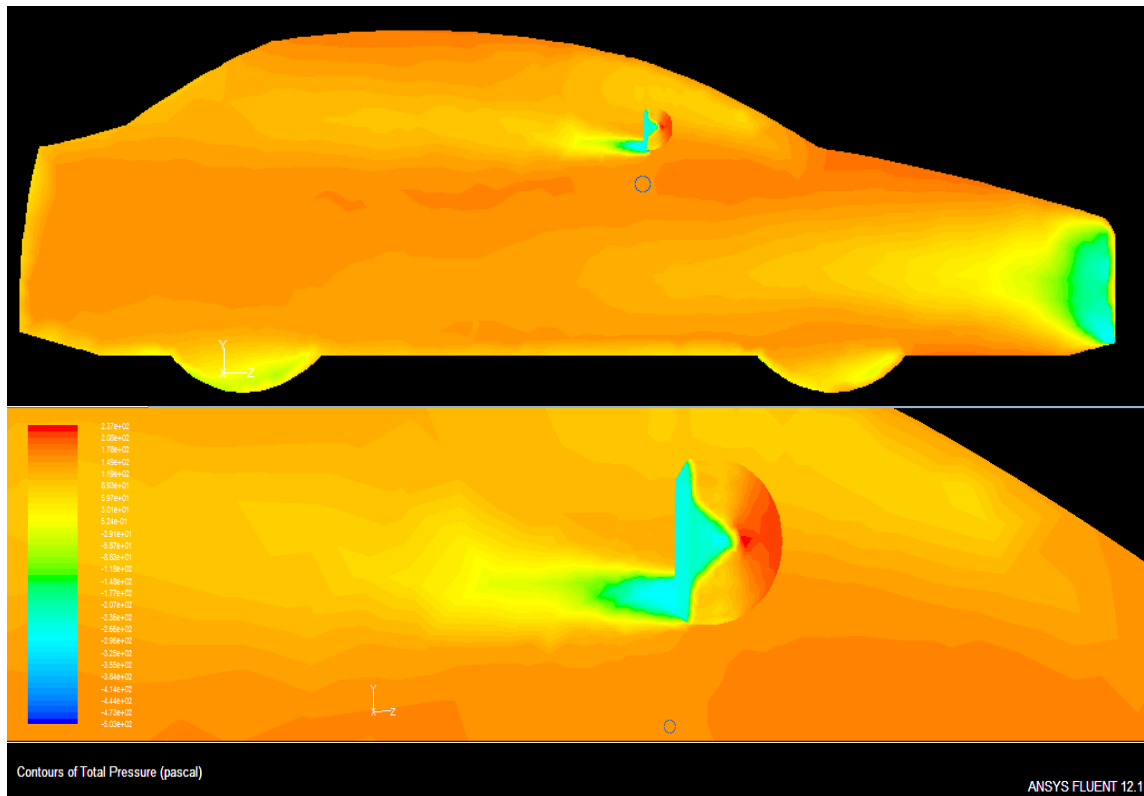


**Figure 4.20:** Total Pressure contour for Model 1 (16.67m/s)

The Figure 4.21 shows the total pressure distribution along the side view of a passenger car using Model 2. Contour colors shows that the total pressure area which has contacts with the side mirror has low pressure contours and the curvature line on the side mirror receives the highest total pressure. This may be caused by the sharp shape of the side mirror. The pressure difference between the side mirror and passenger car body could cause noise and mirror fluctuations.

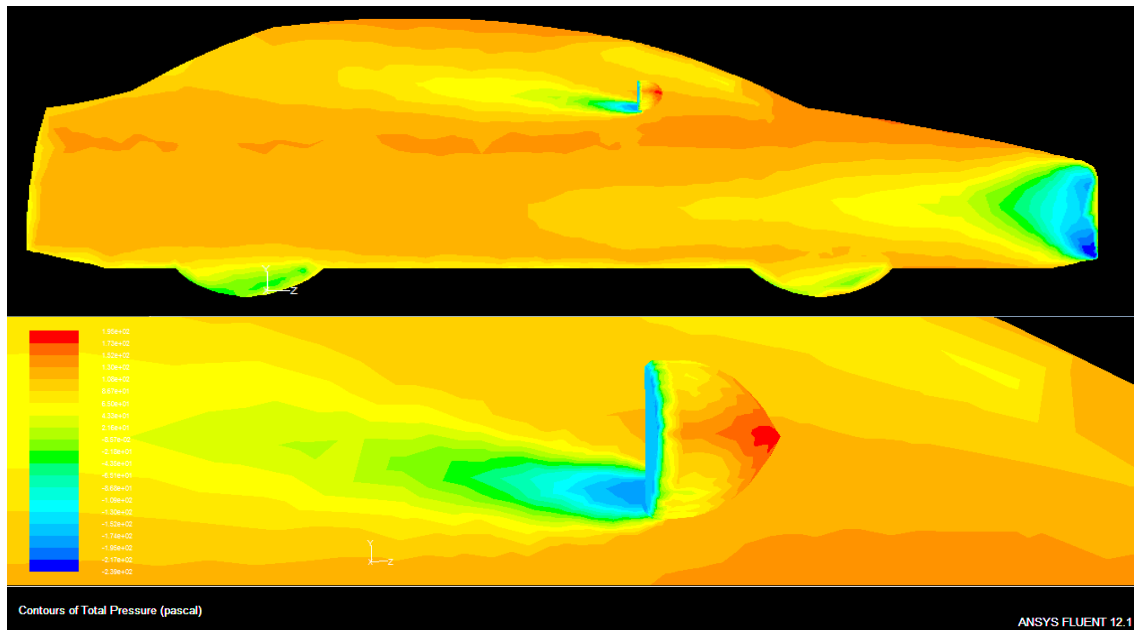


**Figure 4.21:** Total Pressure contour for Model 2 (16.67m/s)

The Figure 4.22 shows the total pressure distribution along the side view of a passenger car. Contour colors show that the total pressure area which is around the side mirror 3 has low pressure coefficient. The high pressure coefficient around the back of the side mirror is due to the frontal contact of the flow.

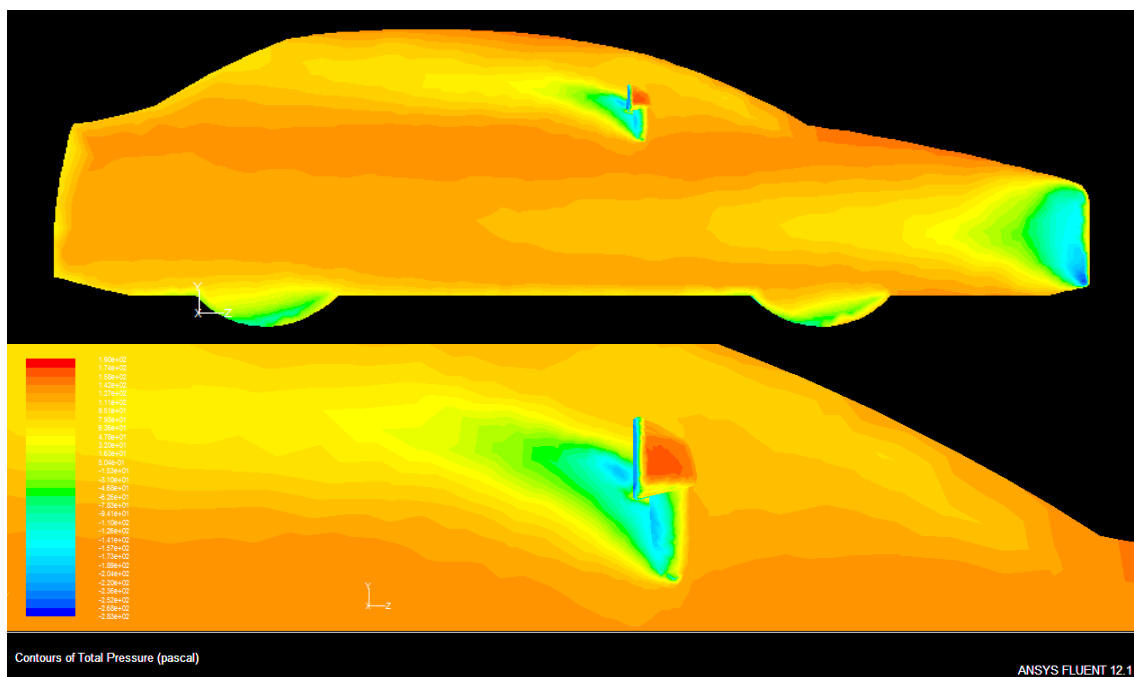


**Figure 4.22:** Total Pressure contour for Model 3 (16.67m/s)

#### 4.4.2 Total Pressure, $P_{\text{Total}}$ for 25m/s (90km/h)

The Figure 4.23 shows the total pressure distribution along the side view of a passenger car. Contour colors shows that the total pressure area which does not contact with the air flow is low while the frontal area of side mirror has high total pressure. This may be caused by the blunt shape of the side mirror. The pressure difference between the side mirror and passenger car body could cause noise and mirror fluctuations.

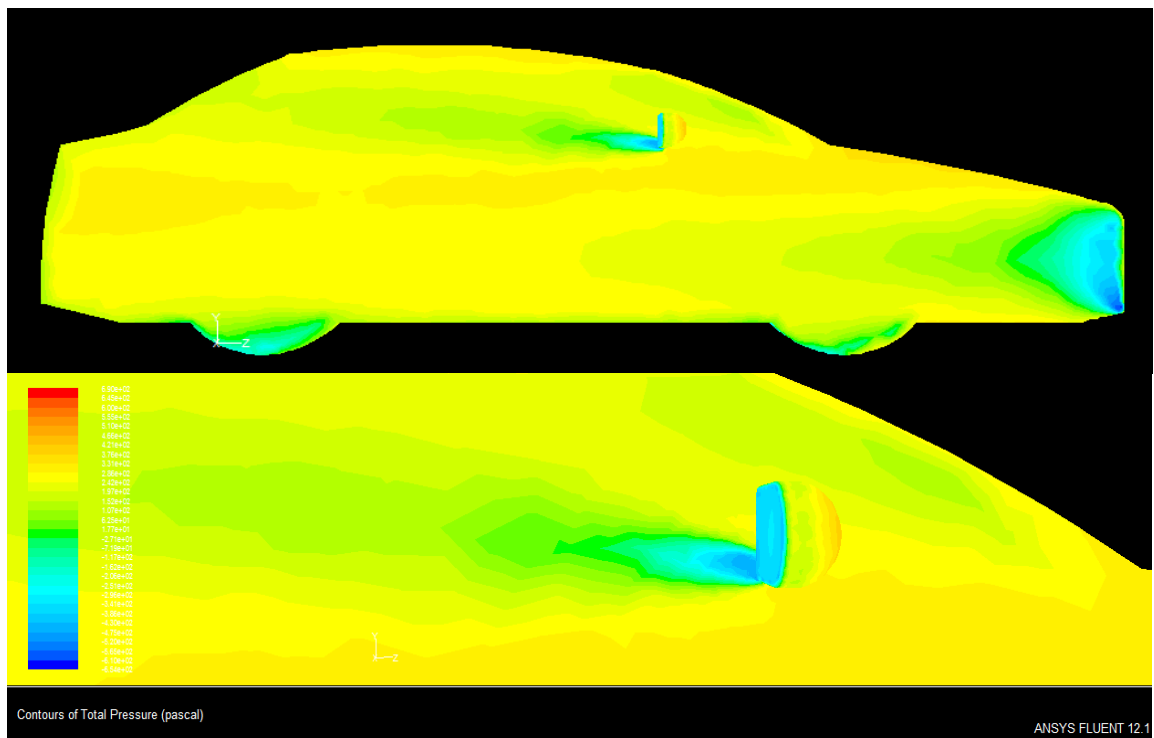


**Figure 4.23:** Total Pressure contour for Model 1 (25m/s)

The Figure 4.24 shows the total pressure distribution along the side view of a passenger car. Contour colors shows that the total pressure area around the driver window is low due to the aerofoil shape of the side mirror. The pressure difference between the side mirror and passenger car body could cause noise and mirror fluctuations.



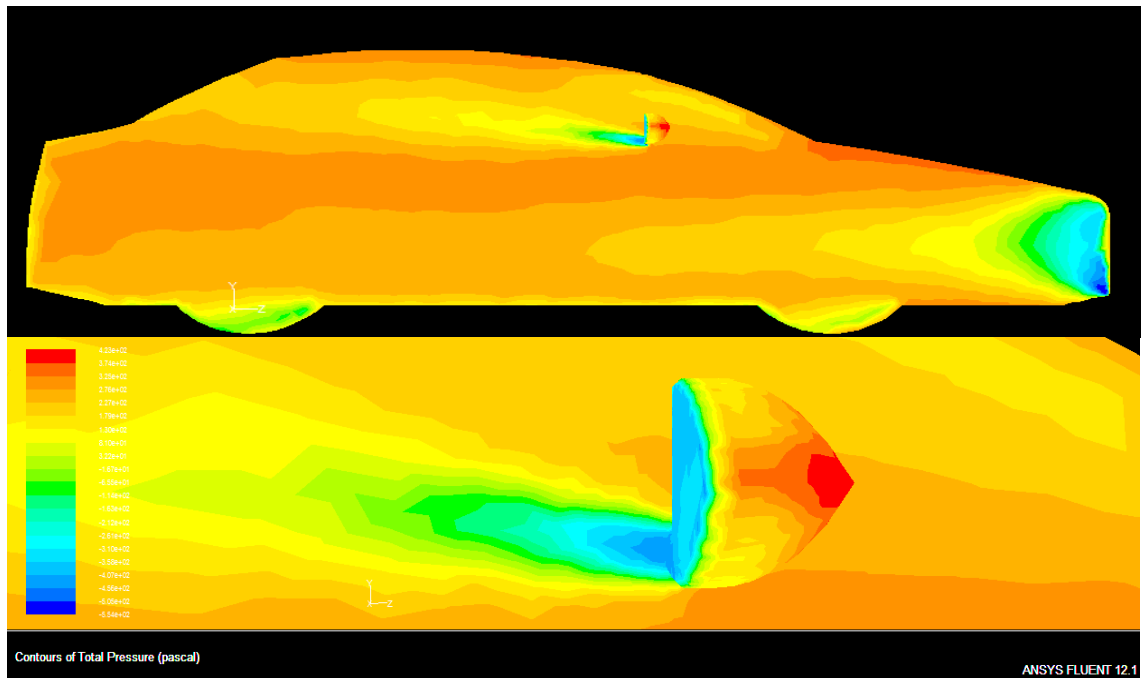


**Figure 4.24:** Total Pressure contour for Model 2 (25m/s)

The Figure 4.25 shows the total pressure distribution along the side view of a passenger car. Contour colors shows that the total pressure area after the flow on side mirror is relatively low due to the small gap between the side mirror and car body. The handle of the side mirror undergoes low pressure coefficient too.

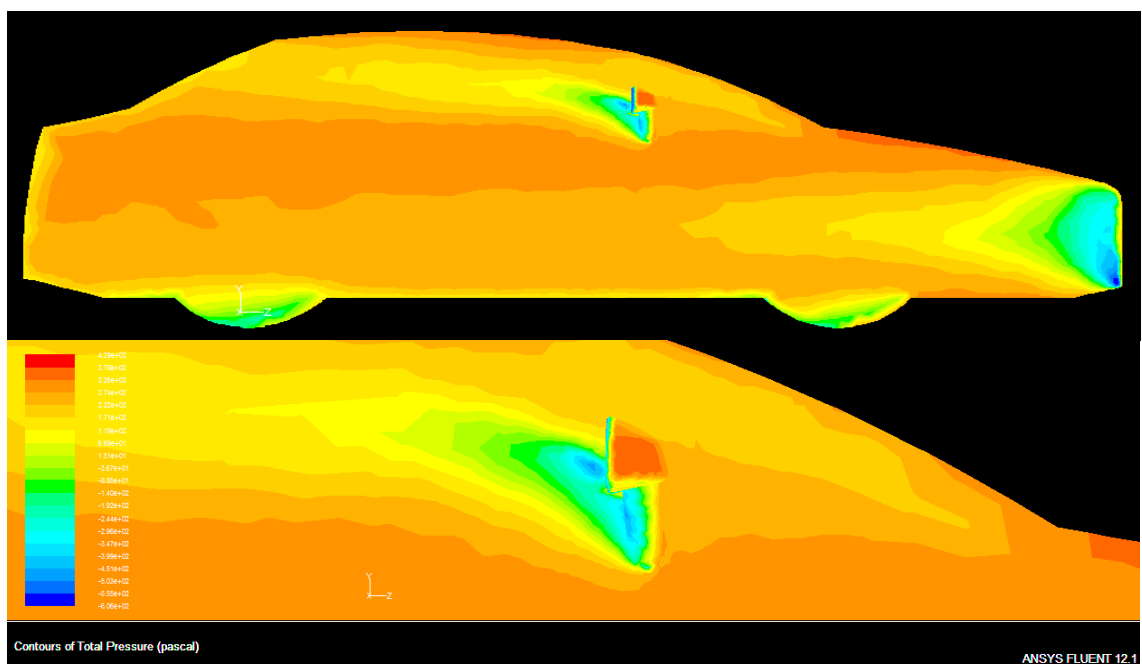


**Figure 4.25:** Total Pressure contour for Model 3 (25m/s)

#### 4.4.3 Total Pressure, $P_{Total}$ for 33.33m/s (120km/h)

The Figure 4.26 shows the total pressure distribution along the side view of a passenger car. Contour colors shows that the total pressure area which does not contact with the air flow is low while the frontal area of side mirror has high total pressure. This may be caused by the blunt shape of the side mirror. The pressure difference between the side mirror and passenger car body could cause noise and mirror fluctuations.

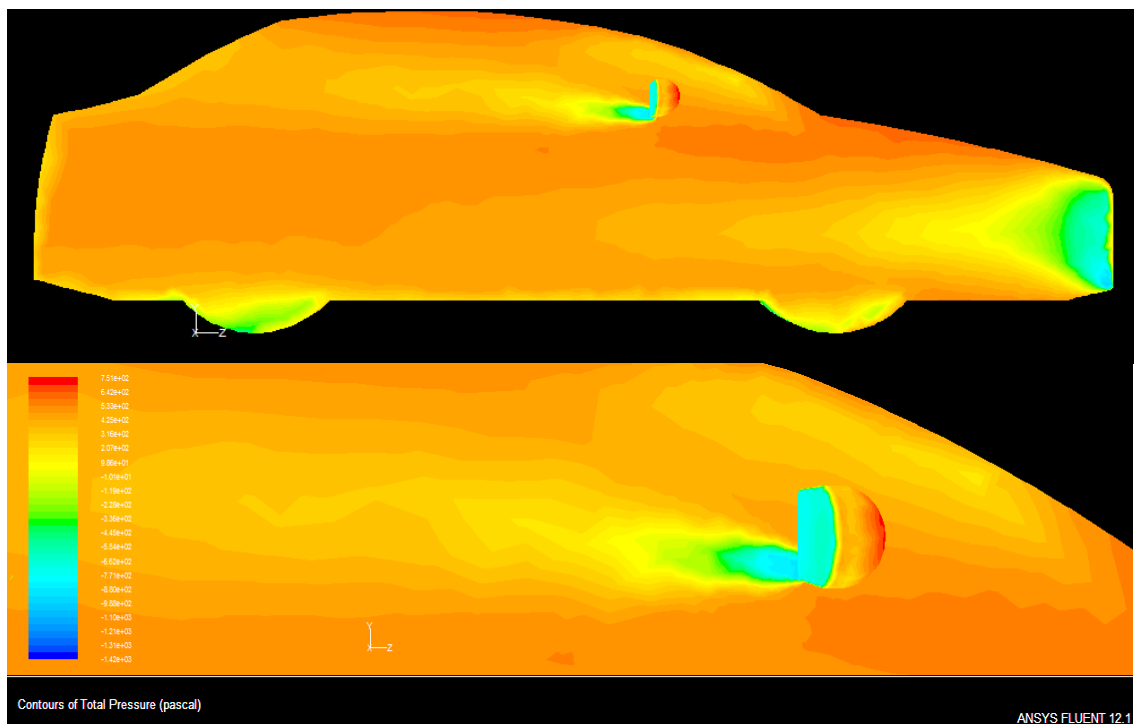


**Figure 4.26:** Total Pressure contour for Model 1 (33.33m/s)

The Figure 4.27 shows the total pressure distribution along the side view of a passenger car. Contour colors shows that in high speed, the total pressure along the driver and passenger is affected the most by the side mirror. The edges around the side mirror receive high turbulence flow that decreases the total pressure around the mirror area. The pressure difference between the side mirror and passenger car body could cause noise and mirror fluctuations.

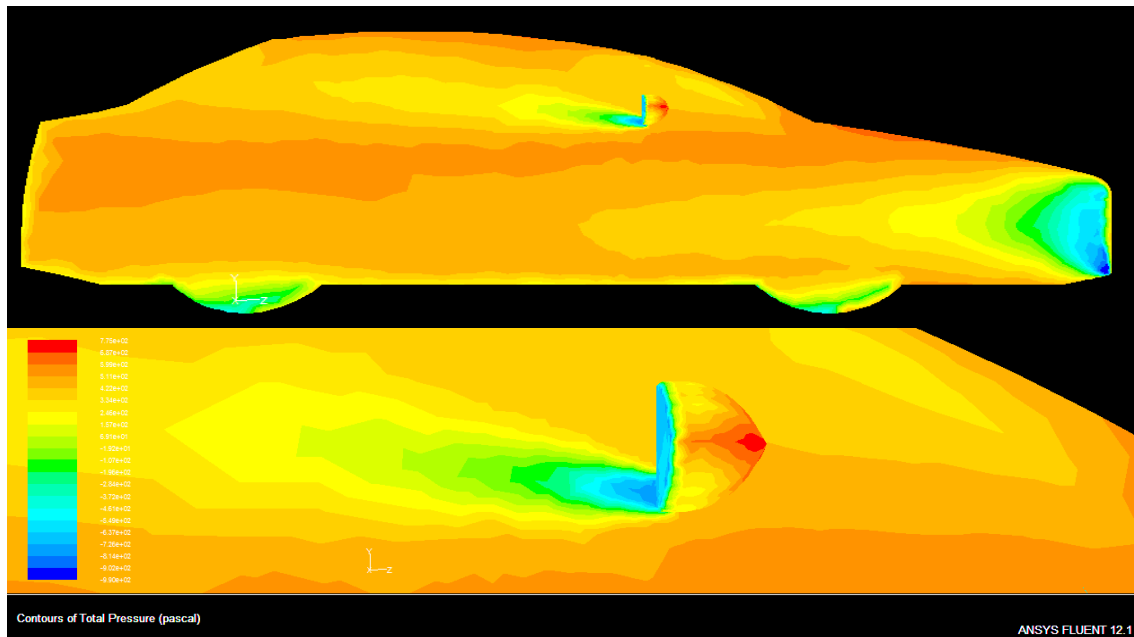


**Figure 4.27:** Total Pressure contour for Model 2 (33.33m/s)

The Figure 4.28 shows the total pressure distribution along the side view of a passenger car. Contour colors shows that the frontal area of the side mirror receives highest pressure coefficient during high speed velocity. Thus, it affects the driver mirror and passenger mirror. The pressure difference between the side mirror and passenger car body could cause noise and mirror fluctuations.

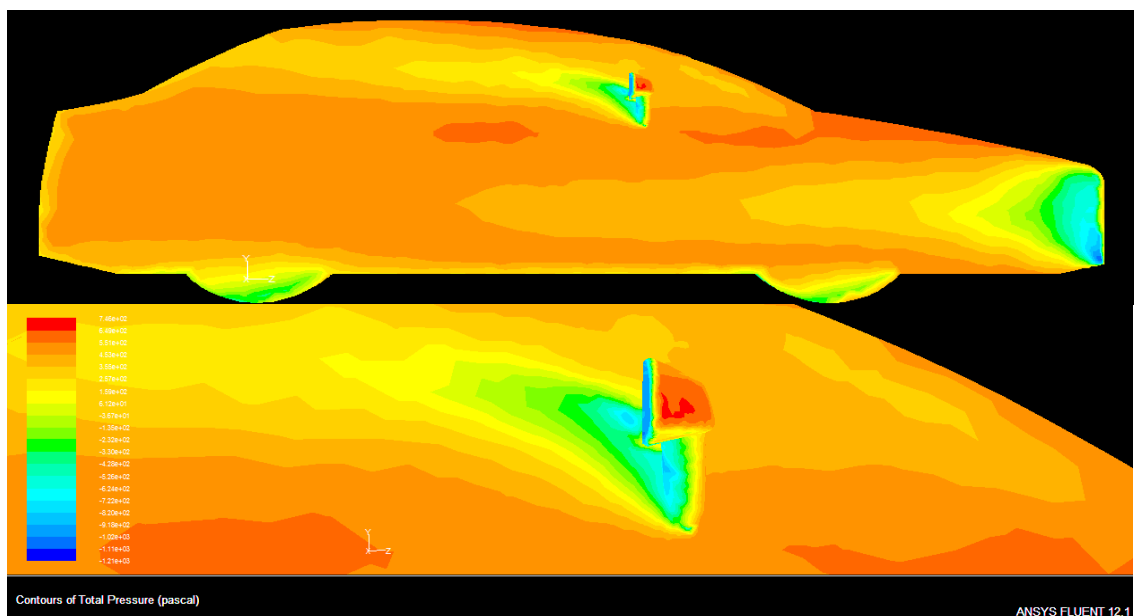


**Figure 4.28:** Total Pressure contour for Model 3 (33.33m/s)

## 4.5 DRAG COEFFICIENT, $C_D$

The component of the resultant aerodynamic force which opposes the forward motion is called the aerodynamic drag. The aerodynamic drag affects the performance of a car in both speed and fuel economy as it is the power required to overcome the opposing force.

The drag coefficient is calculated by generating the drag coefficient graph based on the simulation done using ANSYS Fluent software. The number of iteration used for this calculation is 100 and the final drag coefficient value is taken from the final iteration. The velocity used for the simulation is 16.67m/s (60km/h), 25m/s (90km/h) and 33.33m/s (120km/h).

### 4.5.1 Drag coefficient of side mirror models at 16.67m/s (60km/h)

Based on the Figure 4.29, it shows that the drag coefficient ( $C_d$ ) value for model 1 after simulation is 0.589. The drag coefficient ( $C_d$ ) value for model 2 after simulation is 0.4452. The drag coefficient ( $C_d$ ) value for model 3 after simulation is 0.4476.

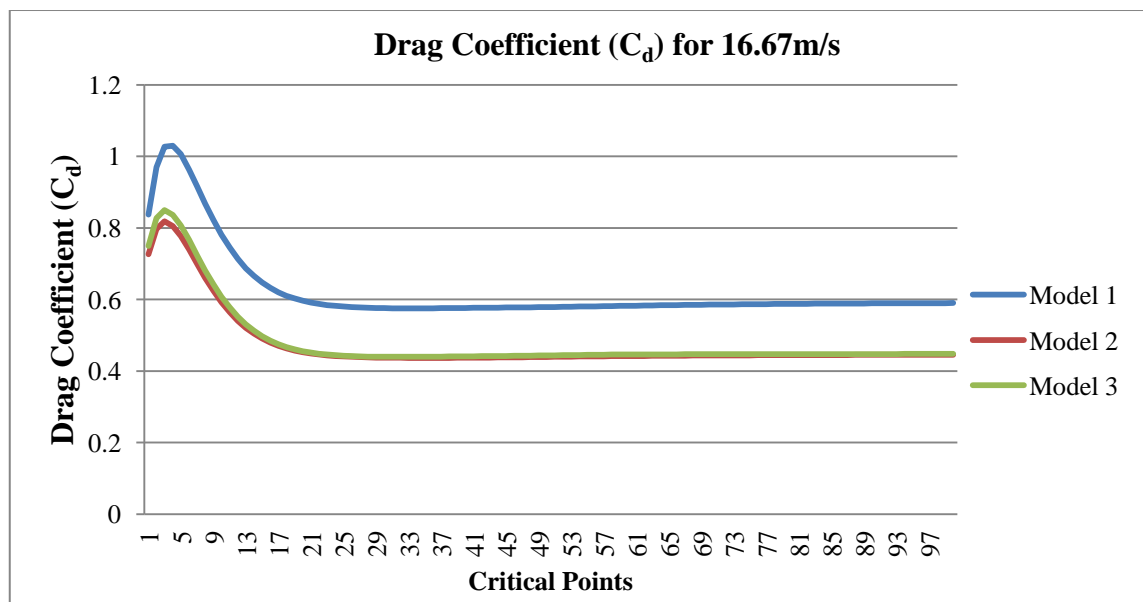


**Figure 4.29:** Graph of Drag coefficient for Models (16.67m/s)

#### 4.5.2 Drag coefficient of side mirror models at 25m/s (90km/h)

Based on the Figure 4.30 below, it shows that the drag coefficient ( $C_d$ ) value for model 1 after simulation is 0.4448. The drag coefficient ( $C_d$ ) value for model 2 after simulation is 0.4485. The drag coefficient ( $C_d$ ) value for model 3 after simulation is 0.4464.

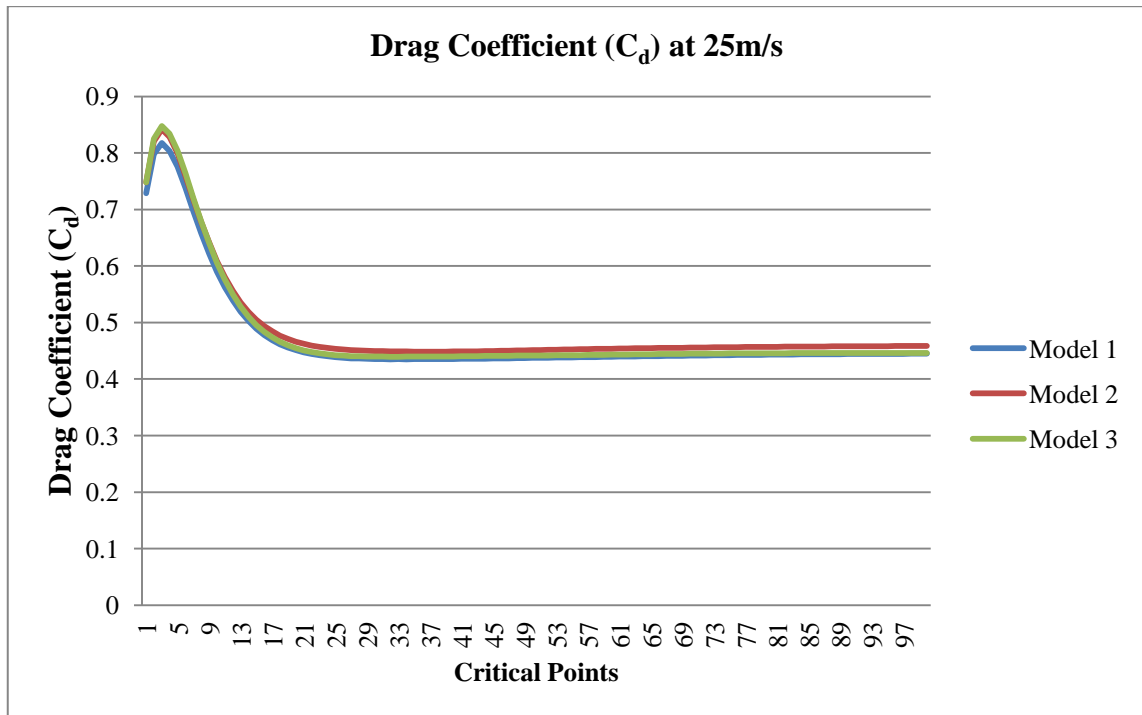


**Figure 4.30:** Graph of Drag coefficient for Models (25m/s)

#### 4.5.3 Drag coefficient of side mirror models at 33.33m/s (120km/h)

Based on the Figure 4.31, it shows that the drag coefficient ( $C_d$ ) value for model 1 after simulation is 0.4438. The drag coefficient ( $C_d$ ) value for model 2 after simulation is 0.4614. The drag coefficient ( $C_d$ ) value for model 3 after simulation is 0.4427.

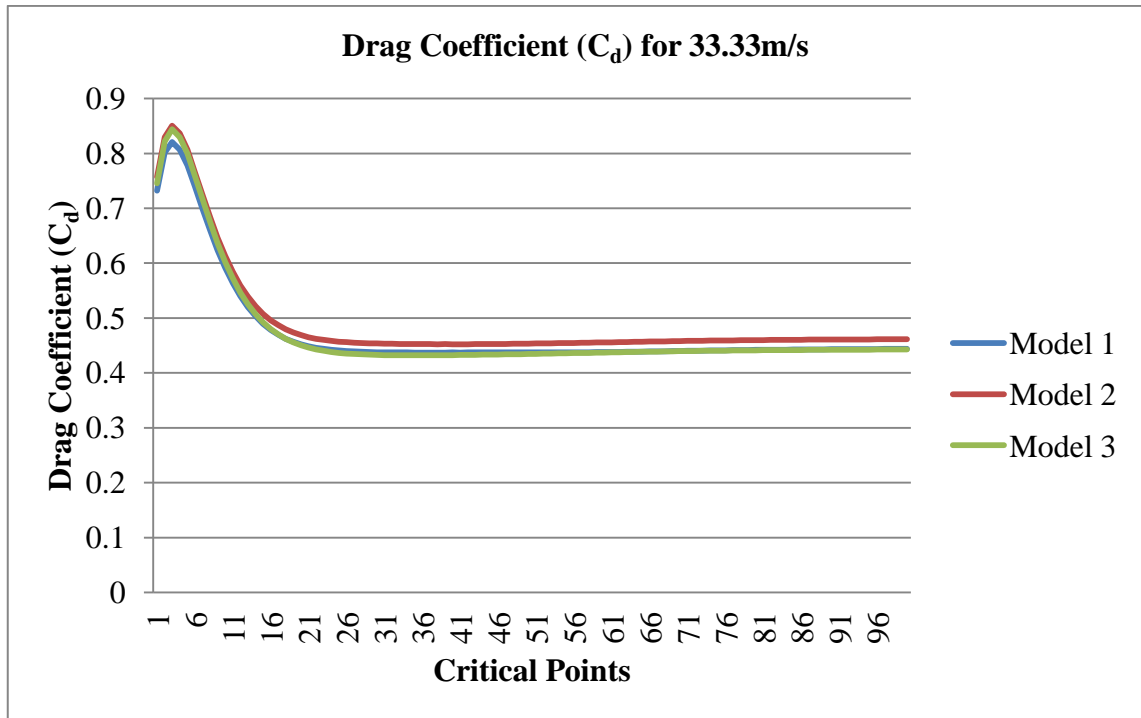


**Figure 4.31:** Graph of Drag coefficient for Models (33.33m/s)

#### 4.6 LIFT COEFFICIENT, $C_L$

Aerodynamic lift and aerodynamic design is one of the key aspects in terms of on-road stability. As long as driving speed is low, below say 120 km/h, lift and pitching moment have only a small effect on the directional stability of a car, even in crosswind. However, at higher speeds this is no longer true, and so recent developments are directed at controlling them.

The lift coefficient is calculated by generating the lift coefficient graph based on the simulation done using ANSYS Fluent software. The number of iteration used for this calculation is 100 and the final lift coefficient value is taken from the final iteration. The velocity used for the simulation is 16.67m/s (60km/h), 25m/s (90km/h) and 33.33m/s (120km/h).

#### 4.6.1 Lift coefficient of side mirror models at 16.67m/s (60km/h)

Based on the Figure 4.32, it shows that the lift coefficient ( $C_L$ ) value for model 1 after simulation is -0.2648. The lift coefficient ( $C_L$ ) value for model 2 after simulation is -0.1958. The lift coefficient ( $C_L$ ) value for model 3 after simulation is -0.0743.

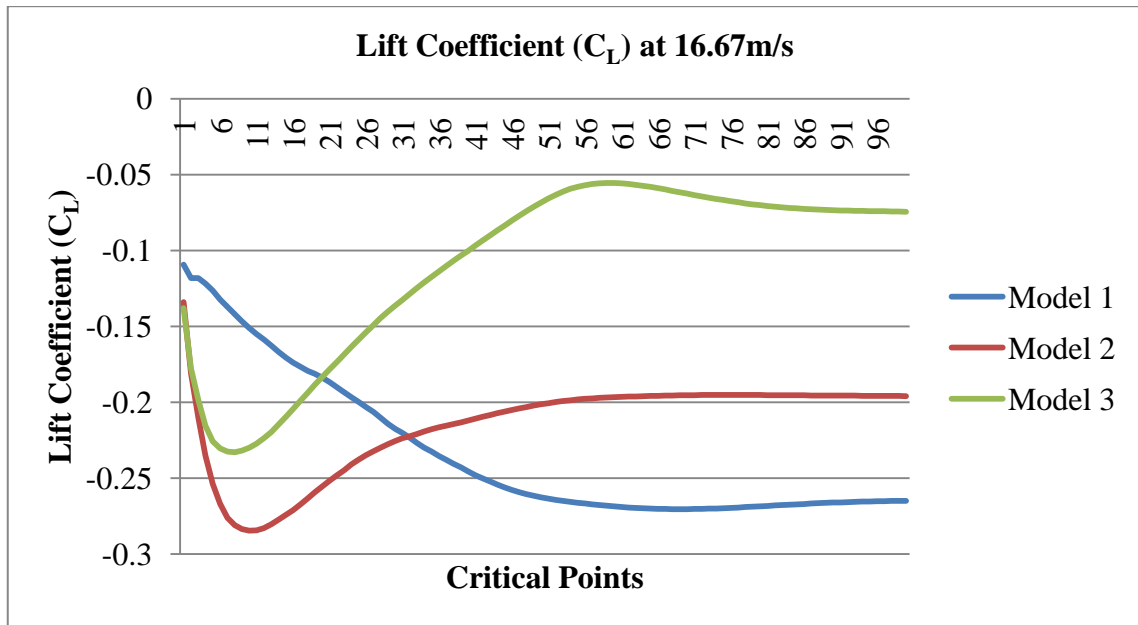


**Figure 4.32:** Graph of Lift coefficient for Models (16.67m/s)

#### 4.6.2 Lift coefficient of side mirror models at 25m/s (90km/h)

Based on the Figure 4.33, it shows that the lift coefficient ( $C_L$ ) value for model 1 after simulation is -0.1102. The lift coefficient ( $C_L$ ) value for model 2 after simulation is -0.2214. The lift coefficient ( $C_L$ ) value for model 3 after simulation is -0.0844.

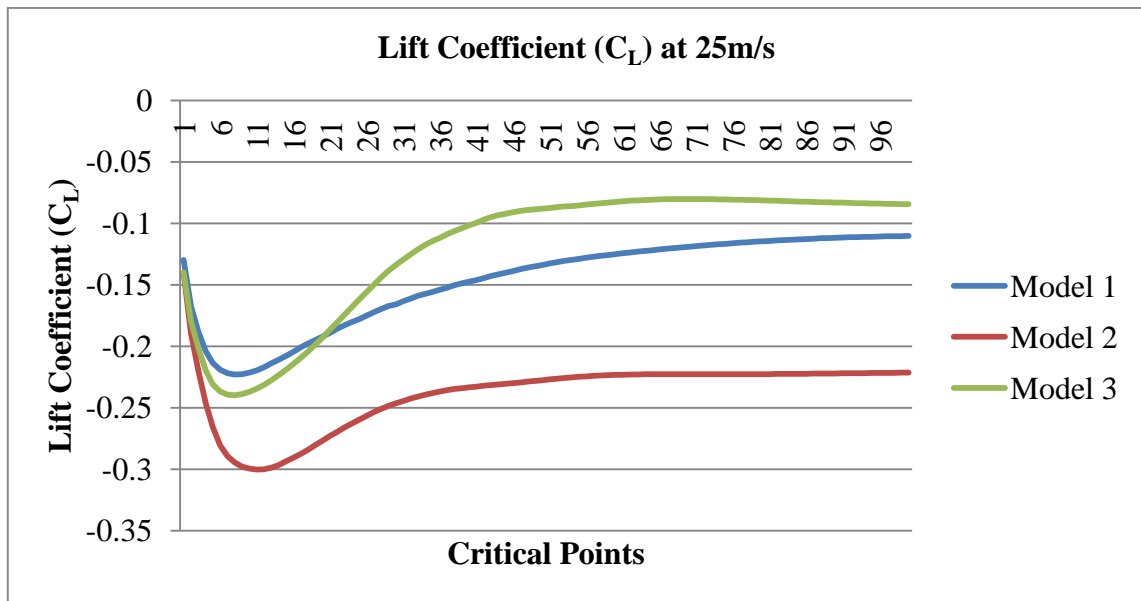


**Figure 4.33:** Graph of Lift coefficient for Models (25m/s)

#### 4.6.3 Lift coefficient of side mirror models at 33.33m/s (120km/h)

Based on the Figure 4.34, it shows that the lift coefficient ( $C_L$ ) value for model 1 after simulation is -0.0911. The lift coefficient ( $C_L$ ) value for model 2 after simulation is -0.1012. The lift coefficient ( $C_L$ ) value for model 3 after simulation is -0.1035.

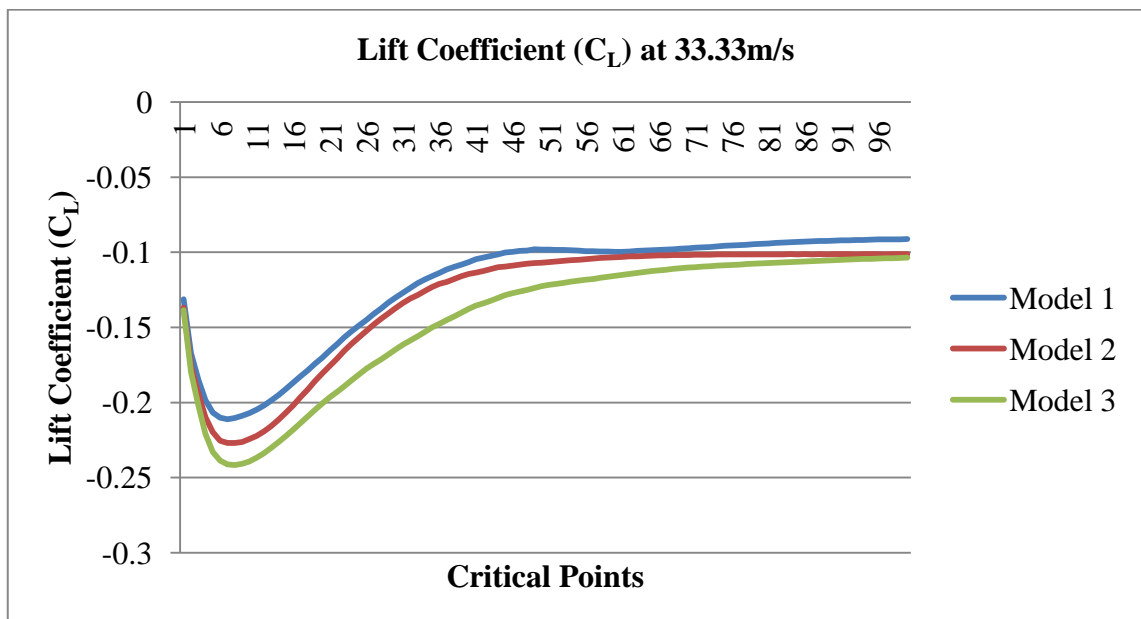


**Figure 4.34:** Graph of Lift coefficient for Models (33.33m/s)



## 4.7 DISCUSSION

Based on the results of drag coefficient and lift coefficient, the designed models are compared and chosen for the best design. Referring to Figure 4.35 below, Model 1 show that the design has low drag coefficient and low lift coefficient at the highest speed which is 33.33m/s while Model 2 has high coefficient and high lift coefficient. Likewise, Model 3 has low drag coefficient but has high lift coefficient. So, the best design that is chosen is Model 1 which has low drag coefficient and low lift coefficient.

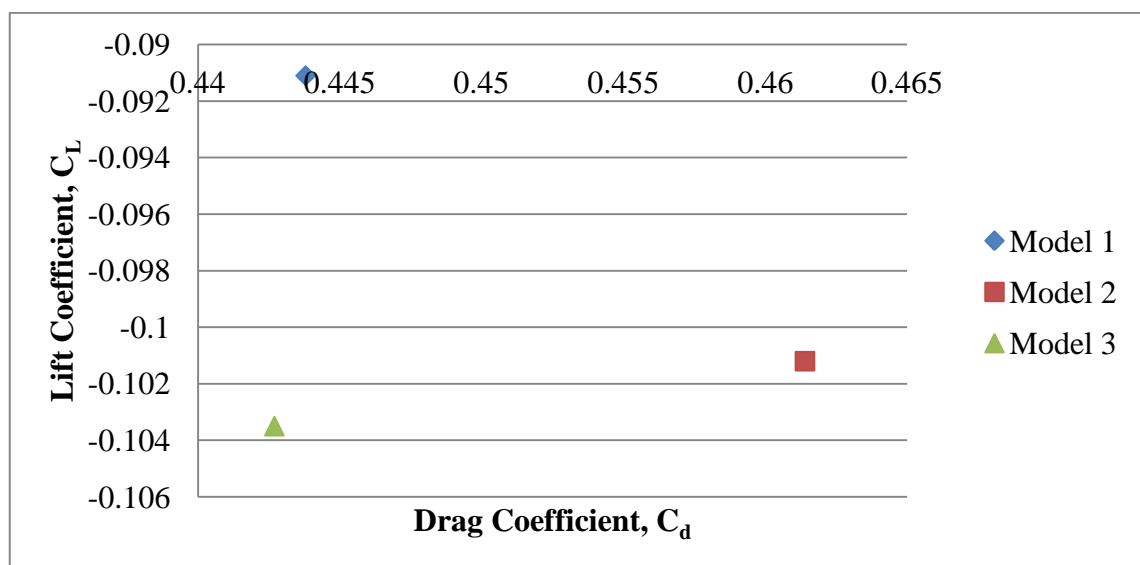


**Figure 4.35:** Design Comparisons at speed of 33.33m/s

## **CHAPTER 5**

### **CONCLUSION AND RECOMMENDATION**

#### **5.1 INTRODUCTION**

The significant findings of the research were concluded in this chapter. The outcome of the research gave overall description of this case study. The limitation or problems encountered during conducting this research also notified together with the recommendations for future research purpose.

#### **5.2 CONCLUSION**

In conclusion, the importance of decreasing the amount of aerodynamics effects and frontal area is because it can influence the fuel consumption, stability and performance.

Before the simulation was done, boundary conditions such as environment pressure and outlet pressure of 1atm are applied. The speed used for the simulation is 16.67m/s (60km/h), 25m/s (90km/h) and 33.33m/s (120km/h). The speed used is same as the experiment method done by F.Alam Et.Al., 2007. Non-slip condition was applied on the entire solid surface.

The discussion done shows the pressure coefficient, total pressure distribution, drag coefficient and lift coefficient value around the car side mirror. Therefore the effect of different side mirrors designs based on the pressure coefficient, drag coefficient and lift coefficient can be estimated. For all the cases, the pressure coefficient around the passenger car was negative but that associated to in front of the side mirror which is

always positive. The CFD simulation of flow over passenger car side mirror was in good agreement with that of the experiment method done by F.Alam Et.Al., 2007.

The comparison of the drag coefficient respectively for the nine cases was studied. All the cases show positive results in a range value of 0.4 to 0.6. The pressure coefficients fluctuate based on the design and speed.

Whereas, lift coefficient show the lift coefficient of the nine cases studied. All the cases show negative results in a range value of -0.05 to -0.3. Side Mirror 3 shows highest drag coefficient with the highest lift coefficient and Side Mirror 1 show the lowest drag coefficient with the smallest lift coefficient. Therefore, Mirror 1 is suitable to be used in passenger cars due to the fuel saving design.

### **5.3 RECOMMENDATIONS FOR FUTURE RESEARCH**

This study provides an overview of computational simulation on a passenger car using different side mirror designs. However, there are some factors which need to be improved to enhance accurate result. The following are some recommendations for future research purpose:

- a) A thorough research of factors affecting the aerodynamic flow should be done
- b) Future experiments involving noise and mirror fluctuation could be done.
- c) To get more accurate results, experimental method should be used and made sure there is no environmental effect towards the results.
- d) Meshing method or grid generation by Finite Volume Method (FVM) or Finite Element Method (FEM) using tetrahedron and not only square meshes.
- e) Transient flow and laminar flow should also be tested.
- f) For more accuracy, error approximation using Taylor series approximation method can be used.

## REFERENCE

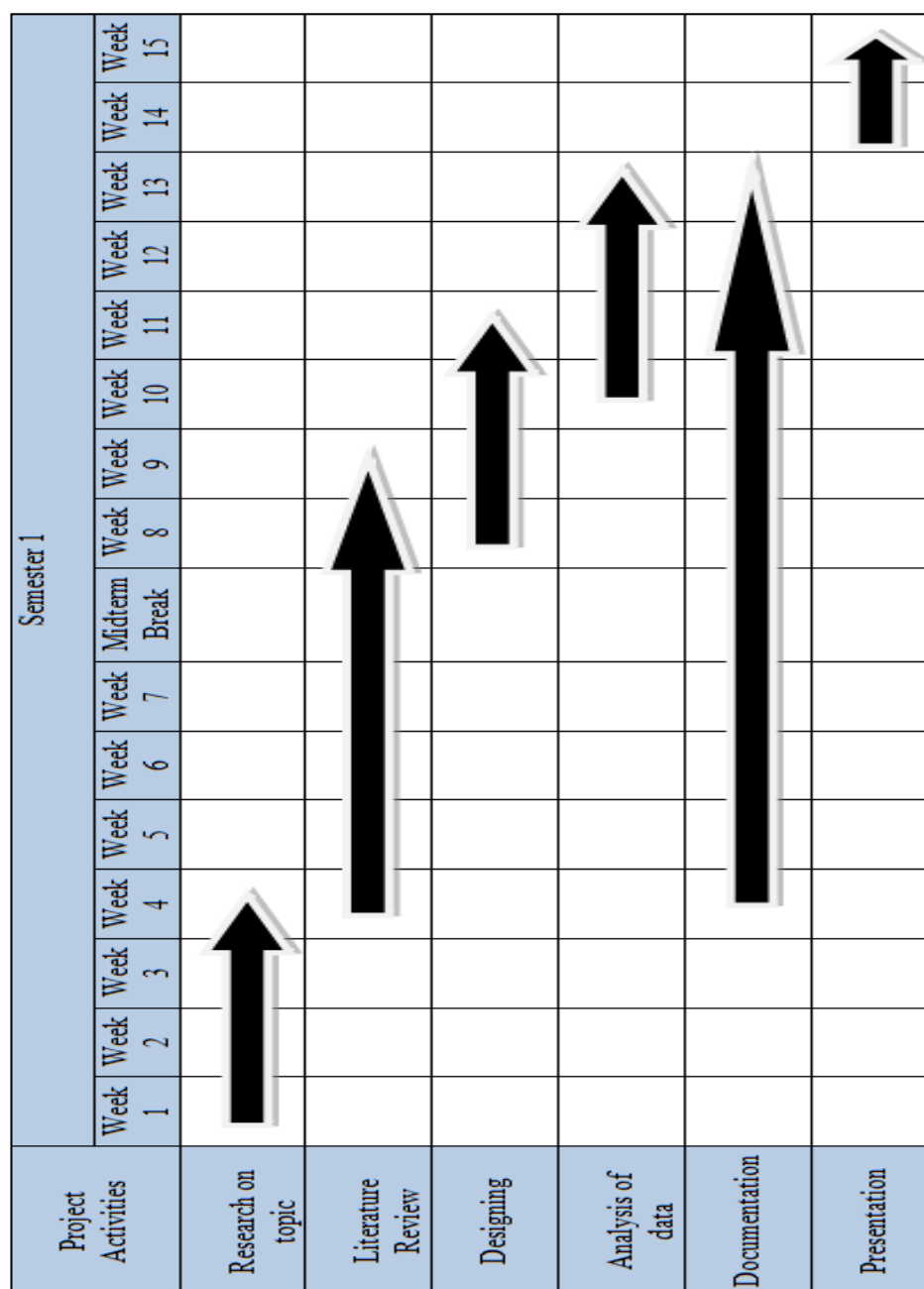
- F. Alam, R. Jaitlee and S. Watkins, *Aerodynamic Effects on an Automotive Rear Side View Mirror*, School of Aerospace, Mechanical and Manufacturing Engineering RMIT University, Melbourne, VIC 3083, AUSTRALIA, **16th Australasian Fluid Mechanics Conference**. 762-765
- Yiping Wang, Zhengqi Gu, Weiping Li and Xiaohui Lin, *Evaluation of Aerodynamic Noise Generation by a Generic Side Mirror*, World Academy of Science, Engineering and Technology **61** 2010. 364-571.
- R. Jaitlee, F. Alam and S. Watkins, Pressure Measurements on an Automobile Side Rear View Mirror, School of Aerospace, Mechanical & Manufacturing Engineering RMIT University, Melbourne, VIC 3083, AUSTRALIA, **15th Australasian Fluid Mechanics Conference**
- Jeong-Hyun Kim, Yong Oun Han, Min Hwa Lee, In Ho Hwang, And Ui Hun Jung, *Surface Flow And Wake Structure Of A Rear View Mirror Of The Passenger Car*, School Of Mechanical Engineering Yeungnam University, Gyeongsan, Gyeongbuk 712-749, Korea, Bbaa Vi International Colloquium On: Bluff Bodies Aerodynamics & Applications.
- Jonas Ask and Lars Davidson, *The Sub-critical Flow past a Generic Side Mirror and its Impact on Sound Generation and Propagation*, **12th AIAA/CEAS Aeroacoustics Conference**, 8-10 May 2006, Cambridge, Massachusetts
- Martin Olsson, *Designing and Optimizing Side-View Mirrors*, Department of Applied Mechanics, Division of Vehicle Engineering and Autonomous Systems, Chalmers University Of Technology.
- A.Yu. Snegirev, S.V. Lupulyak, Yu.K. Shinder, *Use Of High Performance Computing For Simulations Of Aerodynamically Generated Noise In Turbulent Separated Flows*, Laboratory For Applied Mathematics And Mechanics Saint-Petersburg State Polytechnic University Polytechnicheskaya, West-East High Speed Flow Field Conference.
- H. K. Versteeg and W. Malalasekera. *An Introduction to Computational Fluid Dynamics, The Finite Volume Method*. Pearson Prentice Hall, second edition, 2007.
- Thomas D. Gillespie. (2000). *Fundamentals of Vehicle Dynamics*. Pg 74-96
- Yunus A. Cengel, John M.Cimbala. (2006). *Fundamentals of Fluid Mechanics*, 1st Edition in SI Units. Pg 562-600

Michele Ferlauto, Roberto Marsilio, *Computer & Fluids* (2006), *A Viscous Inverse Method for Aerodynamic Design*, pg 304-325

Heisler. H. (2002). *Advanced Vehicle Technology*. Elsevier Butterworth Heinemann, Jordan Hill, Oxford. Pg 121-123

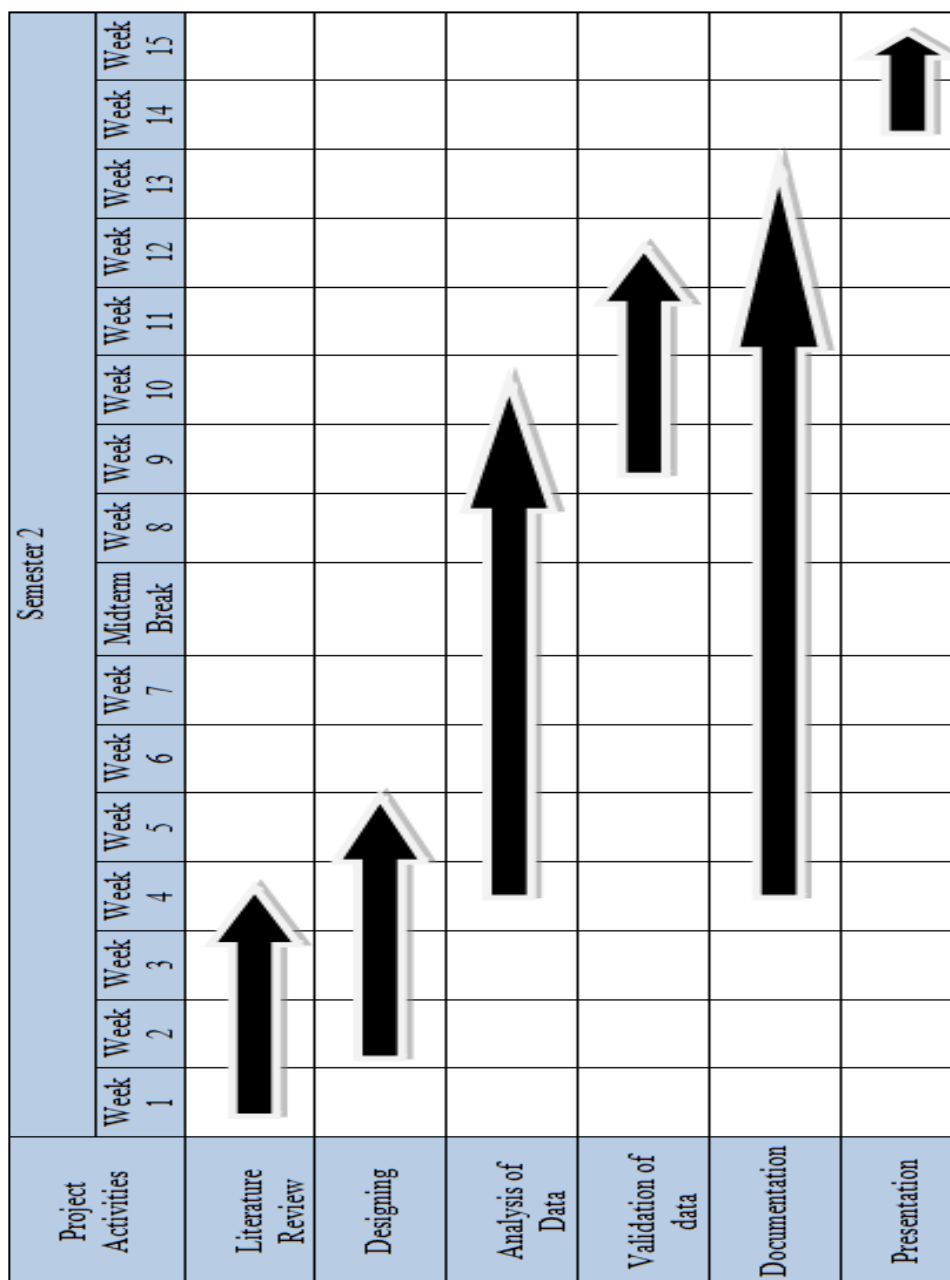
## APPENDIX A1

Gantt chart for Final Year Project 1



## APPENDIX A2

**Gantt chart for Final Year Project 2**



## APPENDIX B1

### Data of Drag Coefficient (16.67m/s)

Model 1	Model 2	Model 3
0.836865	0.726077	0.749162
0.970032	0.796936	0.827258
1.026738	0.818083	0.850202
1.029568	0.804605	0.836246
1.006092	0.776984	0.806563
0.962795	0.739484	0.766435
0.915998	0.698999	0.723064
0.867298	0.659688	0.680656
0.822223	0.623845	0.642041
0.780983	0.591816	0.607442
0.744902	0.564079	0.577383
0.713748	0.540386	0.551715
0.687346	0.520574	0.529983
0.665336	0.504095	0.511981
0.647111	0.490602	0.497048
0.632151	0.479421	0.484932
0.620036	0.470404	0.474938
0.610238	0.463084	0.466966
0.602375	0.457369	0.460575
0.596133	0.452795	0.455572
0.591379	0.449169	0.451537
0.587332	0.44616	0.448393
0.58434	0.443821	0.445968
0.581864	0.442113	0.444084
0.58006	0.440797	0.442668
0.578527	0.43976	0.4416
0.577487	0.438831	0.440825
0.576721	0.438114	0.440276
0.576155	0.437655	0.439935
0.57571	0.437302	0.43972
0.575429	0.437055	0.439636
0.57534	0.436827	0.439646
0.575252	0.436737	0.439745
0.5753	0.43662	0.439852
0.575358	0.436573	0.440015
0.575487	0.436572	0.440168
0.575595	0.436669	0.440364
0.575724	0.436735	0.440533

0.575954	0.436792	0.440718
0.576209	0.436881	0.440883
0.576396	0.437052	0.441122
0.576551	0.437266	0.441348
0.576781	0.437486	0.44159
0.577123	0.437711	0.441802
0.577324	0.437959	0.442065
0.577562	0.438224	0.442359
0.577781	0.438497	0.442657
0.578086	0.438775	0.44293
0.578338	0.439052	0.443225
0.578651	0.439329	0.443554
0.578966	0.439599	0.443892
0.579293	0.439864	0.44422
0.579616	0.440124	0.444535
0.579975	0.440377	0.444835
0.580343	0.440622	0.445114
0.580709	0.440856	0.44536
0.581069	0.441084	0.44557
0.581435	0.441302	0.445755
0.581806	0.441512	0.445915
0.582172	0.441714	0.446059
0.582528	0.441907	0.446182
0.582877	0.442092	0.446289
0.58322	0.44227	0.446376
0.583556	0.442444	0.44646
0.583883	0.44261	0.446532
0.584199	0.442769	0.446598
0.584507	0.442924	0.446644
0.584805	0.443072	0.446693
0.585092	0.443213	0.446739
0.58537	0.443348	0.446785
0.585637	0.443478	0.446821
0.585893	0.443601	0.446862
0.586139	0.443719	0.4469
0.586377	0.443828	0.446939
0.586604	0.443932	0.446974
0.586823	0.444029	0.447014
0.587034	0.44412	0.44705

0.587236	0.444206	0.447085
0.587428	0.444287	0.447119
0.587613	0.444364	0.447156
0.587788	0.444436	0.447188
0.587957	0.444505	0.447219
0.588116	0.444569	0.447247
0.588267	0.444631	0.447281
0.588412	0.444689	0.447309
0.588547	0.444746	0.447336
0.588676	0.4448	0.44736
0.588799	0.444851	0.44739
0.588914	0.4449	0.447413
0.589023	0.444945	0.447436
0.589127	0.44499	0.447457
0.589223	0.445031	0.447484
0.589315	0.445069	0.447507
0.589402	0.445103	0.447529
0.589483	0.445134	0.447552
0.589561	0.445164	0.44758
0.589634	0.445192	0.447606
0.589703	0.445219	0.447629
0.589769	0.445244	0.447653
0.589832	0.445266	0.447679
0.586377	0.443828	0.446939



## APPENDIX B2

### Data of Drag Coefficient (25m/s)

Model 1	Model 2	Model 3
0.729008	0.747983	0.748221
0.798084	0.820606	0.82498
0.817924	0.842312	0.847981
0.803558	0.828299	0.834126
0.7755	0.799747	0.804196
0.737841	0.75877	0.764132
0.697405	0.718103	0.720843
0.65782	0.677835	0.678712
0.622003	0.641336	0.640222
0.590065	0.608552	0.605623
0.562472	0.580345	0.575612
0.538879	0.5561	0.549979
0.519009	0.535779	0.528398
0.502512	0.518785	0.510426
0.488969	0.504907	0.495568
0.477823	0.493505	0.483449
0.468835	0.484411	0.473674
0.461556	0.476947	0.465717
0.455767	0.470973	0.459558
0.451083	0.466121	0.454675
0.447334	0.46241	0.450856
0.444391	0.459353	0.447731
0.442023	0.456981	0.445451
0.440228	0.455073	0.443688
0.438701	0.453626	0.442422
0.437668	0.452418	0.441452
0.436791	0.451504	0.440733
0.436278	0.450834	0.440238
0.435806	0.450269	0.43994
0.435479	0.449796	0.439772
0.435286	0.449361	0.439647
0.435068	0.449135	0.439592
0.435219	0.448937	0.439621
0.435097	0.448796	0.439663
0.435146	0.448627	0.43968
0.435121	0.448617	0.439712

0.435238	0.448627	0.439798
0.435407	0.448682	0.439932
0.43546	0.448693	0.440037
0.435612	0.448814	0.440116
0.435743	0.44894	0.440228
0.435932	0.449084	0.440454
0.43606	0.449247	0.440649
0.436234	0.449454	0.440781
0.436417	0.449717	0.440865
0.436616	0.449963	0.441005
0.436745	0.450263	0.44121
0.436936	0.450527	0.441344
0.437185	0.450872	0.441424
0.43743	0.451163	0.441486
0.437593	0.451487	0.441644
0.437759	0.451755	0.441836
0.438006	0.452065	0.441977
0.438244	0.452338	0.442075
0.438445	0.452609	0.442199
0.438627	0.452844	0.442426
0.438828	0.453096	0.442638
0.43902	0.453329	0.442808
0.439222	0.45355	0.442949
0.43943	0.453756	0.443138
0.439639	0.45397	0.443357
0.43983	0.454177	0.443555
0.440015	0.454374	0.443717
0.440219	0.454566	0.443874
0.44042	0.454759	0.444051
0.440621	0.454949	0.444229
0.440821	0.455135	0.444384
0.44102	0.455313	0.444517
0.441207	0.455486	0.444656
0.441397	0.455655	0.444796
0.441589	0.455819	0.444924
0.441778	0.455975	0.445033
0.441953	0.456126	0.445141

0.44213	0.45627	0.445242
0.442306	0.456408	0.445338
0.442473	0.456541	0.445426
0.442629	0.456669	0.44551
0.442787	0.456792	0.445585
0.442941	0.456911	0.445654
0.443081	0.457025	0.445717
0.443221	0.457134	0.445783
0.443363	0.457239	0.445838
0.443487	0.457341	0.445889
0.443608	0.457439	0.445934
0.443722	0.457534	0.445986
0.443835	0.457625	0.446031
0.443936	0.457714	0.446069
0.444036	0.457799	0.446105
0.444128	0.457882	0.446146
0.444217	0.457961	0.44618
0.4443	0.458037	0.44621
0.444385	0.458111	0.446237
0.444458	0.458182	0.446268
0.444527	0.45825	0.446293
0.444595	0.458316	0.446313
0.444662	0.458378	0.446333
0.444713	0.458437	0.446357
0.444762	0.458493	0.446377
0.444809	0.458546	0.44639
0.444858	0.458596	0.446403

## APPENDIX B3

### Data of Drag Coefficient (33.33m/s)

Model 1	Model 2	Model 3
0.732384	0.757087	0.74524
0.801413	0.829748	0.821934
0.820928	0.850806	0.844127
0.806621	0.836449	0.829678
0.777903	0.806997	0.799849
0.740121	0.765757	0.759755
0.699137	0.724394	0.716809
0.659781	0.68355	0.674813
0.623702	0.64642	0.636541
0.591523	0.613104	0.602137
0.563709	0.584243	0.572263
0.539944	0.559656	0.546671
0.519929	0.538921	0.525071
0.503338	0.521768	0.507053
0.489674	0.507559	0.492117
0.478516	0.496092	0.479967
0.469495	0.486916	0.470026
0.462323	0.479454	0.461932
0.45667	0.473549	0.455418
0.452161	0.468795	0.450286
0.448531	0.465203	0.446171
0.445749	0.462318	0.442836
0.443732	0.460071	0.440271
0.442143	0.458279	0.438269
0.440853	0.456975	0.436658
0.43975	0.456009	0.435345
0.439037	0.45517	0.434446
0.438523	0.454462	0.433889
0.438115	0.453983	0.433364
0.437754	0.453732	0.432853
0.437533	0.453378	0.432519
0.437435	0.453051	0.432398
0.437336	0.452839	0.432361
0.437262	0.452735	0.432297
0.437179	0.452669	0.432134
0.437197	0.452479	0.432183
0.437163	0.45244	0.432284
0.437223	0.45235	0.432416

0.437243	0.452457	0.432533
0.437261	0.452352	0.432519
0.437251	0.452379	0.432681
0.437352	0.452373	0.432887
0.437409	0.452578	0.433054
0.437396	0.452583	0.43323
0.437392	0.452669	0.433444
0.437465	0.452757	0.43367
0.437515	0.452969	0.433884
0.437468	0.45305	0.43403
0.437435	0.453206	0.434289
0.437481	0.453393	0.434588
0.437526	0.453638	0.434833
0.437475	0.453781	0.434994
0.437456	0.453985	0.435206
0.437503	0.454203	0.435548
0.437569	0.454479	0.435856
0.437585	0.454706	0.436092
0.437647	0.454937	0.43629
0.437775	0.455169	0.43657
0.437906	0.455425	0.436923
0.438008	0.455669	0.437217
0.438144	0.455913	0.437449
0.438319	0.456156	0.437678
0.438495	0.456408	0.437976
0.43867	0.456649	0.438279
0.438859	0.456892	0.438534
0.43909	0.457132	0.438746
0.439309	0.457373	0.438975
0.439515	0.457601	0.439229
0.439717	0.457827	0.439476
0.439947	0.458049	0.439684
0.440183	0.458268	0.439875
0.440385	0.458472	0.440063
0.440593	0.458676	0.440262
0.440811	0.458869	0.440447
0.441025	0.459058	0.440608
0.441214	0.45923	0.440754
0.441403	0.459397	0.440903

0.441586	0.459556	0.441051
0.44177	0.459707	0.441186
0.441925	0.459843	0.441301
0.442079	0.459975	0.441415
0.442226	0.460098	0.441524
0.442378	0.460216	0.441628
0.442504	0.460321	0.44172
0.442626	0.460425	0.441808
0.442743	0.460523	0.44189
0.442866	0.460615	0.441972
0.442966	0.460697	0.442044
0.44306	0.460777	0.442115
0.44315	0.460853	0.442182
0.44325	0.460926	0.442245
0.443334	0.460989	0.442309
0.443408	0.46105	0.442372
0.443479	0.461112	0.442432
0.44356	0.461168	0.442489
0.443628	0.461219	0.442539
0.44369	0.461269	0.442593
0.443749	0.461319	0.442643
0.443816	0.461366	0.442687
0.443877	0.461409	0.442729

## APPENDIX C1

### Data of Lift Coefficient (16.67m/s)

Model 1	Model 2	Model 3
-0.10917	-0.13394	-0.13794
-0.11804	-0.18071	-0.17762
-0.1182	-0.20999	-0.19858
-0.12165	-0.2349	-0.21546
-0.12633	-0.25373	-0.22564
-0.13219	-0.26682	-0.23035
-0.13707	-0.27602	-0.23249
-0.14196	-0.28093	-0.23281
-0.14665	-0.28359	-0.23189
-0.15106	-0.28461	-0.22996
-0.15494	-0.28431	-0.22721
-0.1587	-0.28279	-0.22359
-0.16259	-0.28027	-0.21961
-0.16664	-0.27742	-0.21467
-0.1704	-0.27421	-0.20975
-0.17379	-0.27097	-0.20431
-0.17648	-0.26721	-0.19891
-0.17921	-0.26325	-0.19353
-0.18128	-0.25915	-0.1884
-0.18379	-0.25537	-0.1832
-0.18658	-0.25166	-0.1782
-0.19015	-0.24806	-0.17339
-0.19339	-0.24459	-0.16837
-0.19667	-0.24099	-0.16339
-0.1998	-0.23768	-0.15854
-0.20303	-0.2347	-0.1538
-0.20638	-0.23224	-0.14906
-0.21014	-0.22999	-0.14457
-0.214	-0.22758	-0.14036
-0.21742	-0.2254	-0.1363
-0.22028	-0.22357	-0.13238
-0.22348	-0.22222	-0.12853
-0.22675	-0.22077	-0.12463
-0.22985	-0.21916	-0.1208
-0.23239	-0.21764	-0.11716
-0.23533	-0.21639	-0.11369

-0.23796	-0.2153	-0.11015
-0.24056	-0.21425	-0.10675
-0.24289	-0.21316	-0.10337
-0.24558	-0.21194	-0.10009
-0.24802	-0.21067	-0.09667
-0.25011	-0.20945	-0.09332
-0.25207	-0.20829	-0.08997
-0.25408	-0.2072	-0.08675
-0.25608	-0.20611	-0.08349
-0.25775	-0.20504	-0.0802
-0.25923	-0.204	-0.07705
-0.26046	-0.20303	-0.0741
-0.26158	-0.20213	-0.07112
-0.26259	-0.20131	-0.06827
-0.26351	-0.20055	-0.06561
-0.26429	-0.19985	-0.06324
-0.26496	-0.19921	-0.06113
-0.26558	-0.19864	-0.05935
-0.26616	-0.19816	-0.05799
-0.26671	-0.19774	-0.05694
-0.2672	-0.19738	-0.05614
-0.26768	-0.19708	-0.05568
-0.26815	-0.19683	-0.05551
-0.26858	-0.19661	-0.05552
-0.26897	-0.19642	-0.0557
-0.2693	-0.19625	-0.05611
-0.26959	-0.19609	-0.05669
-0.26984	-0.19595	-0.05735
-0.27002	-0.19581	-0.05803
-0.27017	-0.19569	-0.05882
-0.27027	-0.19559	-0.05975
-0.27032	-0.19549	-0.06066
-0.27034	-0.1954	-0.06152
-0.27033	-0.19532	-0.06243
-0.27027	-0.19526	-0.06337
-0.27018	-0.19521	-0.06425
-0.27005	-0.19517	-0.06507

-0.2699	-0.19514	-0.06591
-0.26971	-0.19513	-0.0667
-0.2695	-0.19513	-0.06742
-0.26928	-0.19514	-0.06814
-0.26903	-0.19516	-0.06885
-0.26877	-0.19518	-0.06949
-0.26851	-0.19521	-0.07004
-0.26825	-0.19524	-0.07054
-0.26798	-0.19528	-0.07107
-0.26771	-0.19531	-0.07154
-0.26745	-0.19534	-0.07189
-0.26719	-0.19537	-0.07221
-0.26695	-0.1954	-0.07254
-0.26672	-0.19543	-0.07281
-0.2665	-0.19545	-0.07301
-0.26629	-0.19548	-0.0732
-0.26609	-0.19551	-0.07339
-0.26591	-0.19554	-0.07355
-0.26574	-0.19557	-0.07366
-0.26559	-0.1956	-0.07375
-0.26545	-0.19564	-0.07388
-0.26533	-0.19568	-0.07399
-0.26522	-0.19572	-0.07405
-0.26512	-0.19576	-0.07411
-0.26502	-0.1958	-0.07421
-0.26495	-0.19585	-0.07431
-0.26487	-0.19589	-0.07437

## APPENDIX C2

### Data of Lift Coefficient (25m/s)

Model 1	Model 2	Model 3
-0.12965	-0.14002	-0.13974
-0.16731	-0.18958	-0.17982
-0.18796	-0.21987	-0.20126
-0.20383	-0.24612	-0.21962
-0.21369	-0.2657	-0.23109
-0.21903	-0.28048	-0.23676
-0.22197	-0.28933	-0.23932
-0.22296	-0.29466	-0.23984
-0.22282	-0.29789	-0.23891
-0.22145	-0.29963	-0.23705
-0.21949	-0.3003	-0.23443
-0.21691	-0.30013	-0.23133
-0.21392	-0.29876	-0.22761
-0.21108	-0.29668	-0.22337
-0.20783	-0.29349	-0.21899
-0.20449	-0.29066	-0.2144
-0.20083	-0.28747	-0.20937
-0.19768	-0.28423	-0.20417
-0.19485	-0.28037	-0.19848
-0.19205	-0.27674	-0.19263
-0.18899	-0.27307	-0.18661
-0.18565	-0.26962	-0.1805
-0.18292	-0.26608	-0.17432
-0.18036	-0.26282	-0.16794
-0.17802	-0.25969	-0.16179
-0.17491	-0.25648	-0.1557
-0.17204	-0.25351	-0.14964
-0.16955	-0.2508	-0.14386
-0.1673	-0.24858	-0.13861
-0.16579	-0.24634	-0.1339
-0.16322	-0.24446	-0.12953
-0.1612	-0.24258	-0.12524
-0.15885	-0.24098	-0.12112
-0.15721	-0.23935	-0.11748
-0.15568	-0.23809	-0.11445
-0.15383	-0.23683	-0.11168

-0.15225	-0.2358	-0.10894
-0.15035	-0.23479	-0.10625
-0.14878	-0.23405	-0.10386
-0.14739	-0.23332	-0.10163
-0.14617	-0.23274	-0.09939
-0.14461	-0.23215	-0.09698
-0.14281	-0.23163	-0.09487
-0.14131	-0.23106	-0.09332
-0.14007	-0.23053	-0.09213
-0.13874	-0.23002	-0.09093
-0.13728	-0.22941	-0.08984
-0.13592	-0.22877	-0.08912
-0.13483	-0.22811	-0.08864
-0.13374	-0.22754	-0.08805
-0.13257	-0.2269	-0.08743
-0.13149	-0.22631	-0.08681
-0.13053	-0.22573	-0.08632
-0.12968	-0.22526	-0.08581
-0.12882	-0.22482	-0.08531
-0.12796	-0.22443	-0.08471
-0.12716	-0.22408	-0.08409
-0.1264	-0.22379	-0.08348
-0.12569	-0.22353	-0.08299
-0.12496	-0.2233	-0.08254
-0.1243	-0.22313	-0.08202
-0.12366	-0.22299	-0.0815
-0.12299	-0.22288	-0.08116
-0.1223	-0.22279	-0.08095
-0.12175	-0.22273	-0.08067
-0.12122	-0.22269	-0.08039
-0.12058	-0.22267	-0.08026
-0.11996	-0.22264	-0.08023
-0.11948	-0.22264	-0.08014
-0.11899	-0.22263	-0.08007
-0.11839	-0.22264	-0.08012
-0.11792	-0.22264	-0.08021
-0.11749	-0.22265	-0.08026

-0.11703	-0.22266	-0.08036
-0.11654	-0.22267	-0.08052
-0.1161	-0.22268	-0.08066
-0.11572	-0.22267	-0.08077
-0.11535	-0.22266	-0.08088
-0.11494	-0.22264	-0.08108
-0.11459	-0.22261	-0.08126
-0.11423	-0.22258	-0.08139
-0.11384	-0.22254	-0.08155
-0.11351	-0.2225	-0.0818
-0.11321	-0.22245	-0.08201
-0.11289	-0.2224	-0.08215
-0.11264	-0.22234	-0.0823
-0.1124	-0.22228	-0.08253
-0.1121	-0.22221	-0.08273
-0.11189	-0.22215	-0.08285
-0.11176	-0.22208	-0.08299
-0.11157	-0.22201	-0.08319
-0.11128	-0.22194	-0.08335
-0.11112	-0.22187	-0.08346
-0.11103	-0.2218	-0.08357
-0.11084	-0.22174	-0.08376
-0.11061	-0.22168	-0.08392
-0.11053	-0.22162	-0.08402
-0.11048	-0.22156	-0.08411
-0.11033	-0.22151	-0.08429

## APPENDIX C3

### Data of Lift Coefficient (33.33m/s)

Model 1	Model 2	Model 3
-0.1313	-0.13671	-0.13845
-0.16702	-0.17531	-0.17951
-0.18474	-0.19391	-0.20184
-0.1983	-0.20961	-0.22067
-0.20672	-0.21968	-0.2329
-0.21002	-0.22548	-0.2387
-0.21106	-0.22686	-0.24128
-0.2104	-0.22695	-0.24157
-0.20889	-0.22622	-0.2407
-0.2071	-0.22447	-0.23926
-0.20479	-0.22233	-0.23675
-0.20197	-0.21928	-0.23368
-0.19867	-0.21569	-0.23012
-0.19489	-0.21145	-0.22621
-0.19085	-0.20661	-0.22218
-0.18668	-0.20177	-0.218
-0.18263	-0.19654	-0.21369
-0.17848	-0.19129	-0.20925
-0.17416	-0.18566	-0.20472
-0.16994	-0.18039	-0.20047
-0.16541	-0.17547	-0.19654
-0.16101	-0.17064	-0.19291
-0.15654	-0.16562	-0.18914
-0.15258	-0.16096	-0.18516
-0.14872	-0.15664	-0.18122
-0.14501	-0.15231	-0.17756
-0.14111	-0.148	-0.17435
-0.13732	-0.14431	-0.17128
-0.13362	-0.14082	-0.16805
-0.13019	-0.13713	-0.16466
-0.12699	-0.13372	-0.16154
-0.12368	-0.13091	-0.15872
-0.12054	-0.12849	-0.15586
-0.11795	-0.12575	-0.15291
-0.11587	-0.12307	-0.1501
-0.11372	-0.1211	-0.14756
-0.11147	-0.11968	-0.14509
-0.10967	-0.11791	-0.14277

-0.10812	-0.11582	-0.14018
-0.10645	-0.11432	-0.13765
-0.1047	-0.11359	-0.13551
-0.1036	-0.11256	-0.13399
-0.10251	-0.11115	-0.13239
-0.10134	-0.10996	-0.1304
-0.10005	-0.10942	-0.12851
-0.0996	-0.10896	-0.12716
-0.09903	-0.10829	-0.12609
-0.09877	-0.10756	-0.125
-0.09809	-0.10718	-0.12373
-0.09818	-0.10693	-0.1225
-0.09818	-0.10653	-0.12167
-0.09843	-0.10604	-0.12109
-0.09837	-0.10565	-0.12041
-0.09869	-0.10526	-0.11953
-0.0989	-0.10494	-0.11878
-0.09928	-0.10455	-0.11824
-0.09936	-0.10421	-0.11773
-0.09948	-0.10384	-0.11705
-0.09954	-0.10357	-0.11629
-0.0997	-0.10326	-0.11559
-0.09965	-0.10304	-0.11504
-0.09942	-0.10278	-0.11445
-0.09896	-0.1026	-0.11377
-0.09883	-0.1024	-0.11307
-0.09874	-0.10231	-0.11255
-0.09853	-0.10214	-0.11207
-0.09826	-0.10205	-0.11156
-0.09796	-0.10192	-0.11104
-0.09766	-0.10188	-0.11106
-0.09732	-0.10174	-0.11023
-0.097	-0.1017	-0.10988
-0.09679	-0.1016	-0.10954
-0.09646	-0.10161	-0.10922
-0.09611	-0.10149	-0.10893
-0.09571	-0.10147	-0.10864
-0.09545	-0.10143	-0.10836
-0.09522	-0.10146	-0.10814

-0.09491	-0.10138	-0.10788
-0.09456	-0.10139	-0.10761
-0.09431	-0.10135	-0.10739
-0.09412	-0.10139	-0.1072
-0.09384	-0.10133	-0.10698
-0.09356	-0.10135	-0.10675
-0.09333	-0.10129	-0.10648
-0.09317	-0.10135	-0.10629
-0.09296	-0.10129	-0.10609
-0.09273	-0.1013	-0.10582
-0.09253	-0.10126	-0.10557
-0.0924	-0.10133	-0.10535
-0.09228	-0.10128	-0.10517
-0.0921	-0.10129	-0.10501
-0.09194	-0.10125	-0.10479
-0.09183	-0.1013	-0.10463
-0.09172	-0.10126	-0.10447
-0.09161	-0.10127	-0.10432
-0.09149	-0.10122	-0.10416
-0.0914	-0.1013	-0.10401
-0.09136	-0.10124	-0.10389
-0.09128	-0.10127	-0.10375